Ariel Mission Target Selection: A New Design

Huiyi Wang[a,b], Nicolas B. Cowan[a,b]

[a]Department of Physics, McGill University, 3600 rue University, Montreal, QC H3A 2T8, Canada
[b]Trottier Space Institute; Institute for Research on Exoplanets; Centre for Research in Astrophysics of Quebec

Abstract

The ESA-Ariel mission, designed to be launched in 2029, aims to study thousands of planets by characterizing their atmospheric properties, thermal structure, molecular composition, etc. We present here a new target selection approach for phase curve based on the Ariel short-list provided by Edwards et al. [2019]. To quantify the scientific potential of each prospective target, we devise our own Figure of Merit (FoM) in conjunction with the Ariel Emission Spectroscopy Metric (AESM) and Ariel Transmission Spectroscopy Metric (ATSM). Based on our estimation, we found that full-orbit observation of 51 Tier 2 AESM targets can be observed within 140 days, roughly $\sim 10\%$ of the total mission lifetime. If we allocated 365 days for phase curve investigation and select partial observation of $\pm 45°$ for targets with an orbital period of more than 48 hours, 36 full and 99 partial phase curves could be observed. Notably, this approach is a significant improvement over the previously proposed Ariel phase curve observational strategy (Best in Class) which required more than 5000 days to characterize 43 targets in Tier 2 AESM resolution. We also suggest that within a three year mission timeframe, 524 targets can be observed with transit spectroscopy (60 Tier 3, 95 Tier 2, and 369 Tier 1).

Keywords— phase curve, spectroscopy, transits, eclipses

1 Introduction

In the past decade, the detection of exoplanets has undergone exponential growth, resulting in the discovery of thousands of new planets. This remarkable progress is set to continue with the advent of advanced telescopes such as the Characterising Exoplanet Satellite (CHEOPS, Broeg et al. [2013]), Planetary Transits and Oscillations (PLATO, Rauer et al. [2016]), etc. These telescopes will greatly enhance our understanding of exoplanets by observing numerous transits and facilitating in-depth characterization of their atmospheres.

Before scientists can fully characterize Earth-like planets, a spectroscopy mission is needed

to study atmospheres to refine our knowledge of the thermal structure and molecular composition of those planetary atmospheres. To tackle this, the Atmospheric Remote-sensing Infrared Exoplanet Large-survey (Ariel) is selected as the next ESA medium-class mission. Ariel is a 1-m telescope with simultaneous coverage from $0.5 - 7.8\mu m$. Specifically, the three spectrometers are NIRSpec ($1.1-1.95\mu m$, $R \sim 10$), the AIRS-CH0 ($1.95-3.9\mu m$, $R = 100-200$), and AIRS-CH1 ($3.9-7.8\mu m$, $R = 30 - 60$) [Charnay et al., 2021]. For each observation, the resulting spectrum is binned in wavelength during data analysis to optimize the signal-to-noise (S/N) ratio. Ariel's observational strategy would follow a four-tier approach [Mugnai et al., 2021, Charnay et al., 2021, Tinetti et al., 2021]. Tier 1 observation provides a reconnaissance survey of ~ 1000 targets with S/N ≥ 7. The raw spectra are binned into one spectral point in NIRSpec, two data points in AIRS-CH0, and one data point in AIRS-CH1. This tier would help improve our understanding of the planetary parameters and orbital properties of the planet and refine the mass-radius diagram. For half of the targets, Ariel would provide a Tier 2 observation, with raw data binned at $R = 10, 50, 15$ (75 in total) for NIRSpec, AIRS-CH0, and AIRS-CH1 respectively, with S/N ≥ 7 in each wavelength bin. Tier 2 targets are essential in revealing the atmospheric structure and chemical composition in addition to planetary density, temperature, stellar metalicity, and size. Tier 3 observation provides spectra of about 5 – 10% of the total target, with raw spectral binned at $R = 20, 100, 30$ (150 in total) for each three instruments. Those observations can supply in-depth knowledge of planetary chemistry and dynamics. Tier 4 targets are selected to undergo full or partial phase curve observation for targets of special interest. Phase curves are the time-dependent change in the brightness of an exoplanet observed from Earth during a full orbit [Parmentier and Crossfield, 2018]. Its purpose is to tailor observations of the longitudinal variation in atmospheric dynamics, compositions, thermal structure, heat redistribution, and clouds of exoplanets to complement spectroscopy measurements of transits and eclipses. In Figure 1, we show an example scheme of a transiting planet and its phase curve, which begins and ends with secondary eclipses.

The Ariel mission aims to answer the following science questions [Tinetti et al., 2021, Charnay et al., 2021]:

1. What are the physical processes, including thermal structure, and molecular and chemical

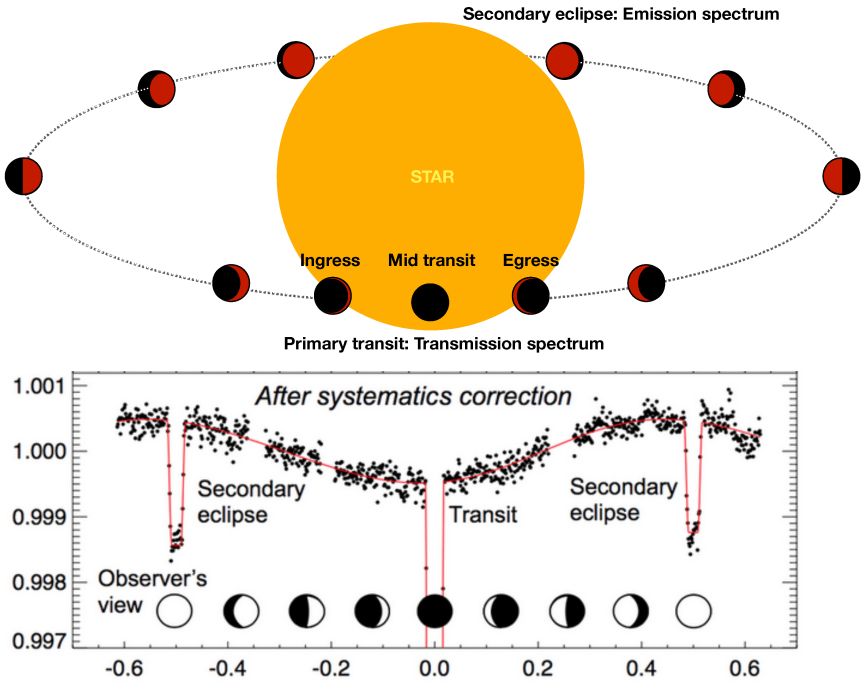

Figure 1: Top: Transiting scheme of an exoplanet around its host star before and after the eclipse. The transit in front of the star is commonly referred to as the primary transit while the eclipse is called the secondary eclipse. **Bottom**: The example phase curve of the exoplanet. Generally, phase curve needs to account for overlapping and includes two eclipses, one at the start and one at the end. Picture not to scale and adapted from Figure 2 of Pluriel [2023], an example phase curve of the hot Jupiter HD 189733 b observed at 4.5 microns with IRAC/Spitzer.

composition, shaping planetary atmosphere?

2. What are exoplanets composed of? How can atmosphere composition help constrain the mass-radius relationship of planets?

3. What is the formation and evolution process of planets and planetary systems?

Hence, it is essential to utilize the four-year scientific lifetime of Ariel maximally to answer those questions. Previously, the ESA-Ariel has planned to dedicate 10% of its mission lifetime to phase curve observations, with 44 targets selected [Charnay et al., 2021] using the Best in Class method. However, this strategy allocates extensive hours to characterize targets with lower signal to ensure planet diversity (discussed in detail in section 3.1). On the other hand, given the launch of JWST, we anticipated that a thorough characterization of numerous phase curve prime targets would have taken place prior to the scheduled launch of Ariel in 2029 with a particular focus on short-period low mass targets, as depicted in Figure 2. Given those circumstances, we propose a

reevaluation of the observational plan for Ariel, with a particular focus on selecting the targets with the most scientific returns in complement to JWST and potentially allocating additional mission time for phase curves. Formerly, Edwards et al. [2019] has produced a short list of 605 Ariel targets mainly for transits and eclipses. In this project, we build on this short-list and select the optimal targets for phase curve observation to maximize the scientific output by constructing our own Figure of Merit (FoM).

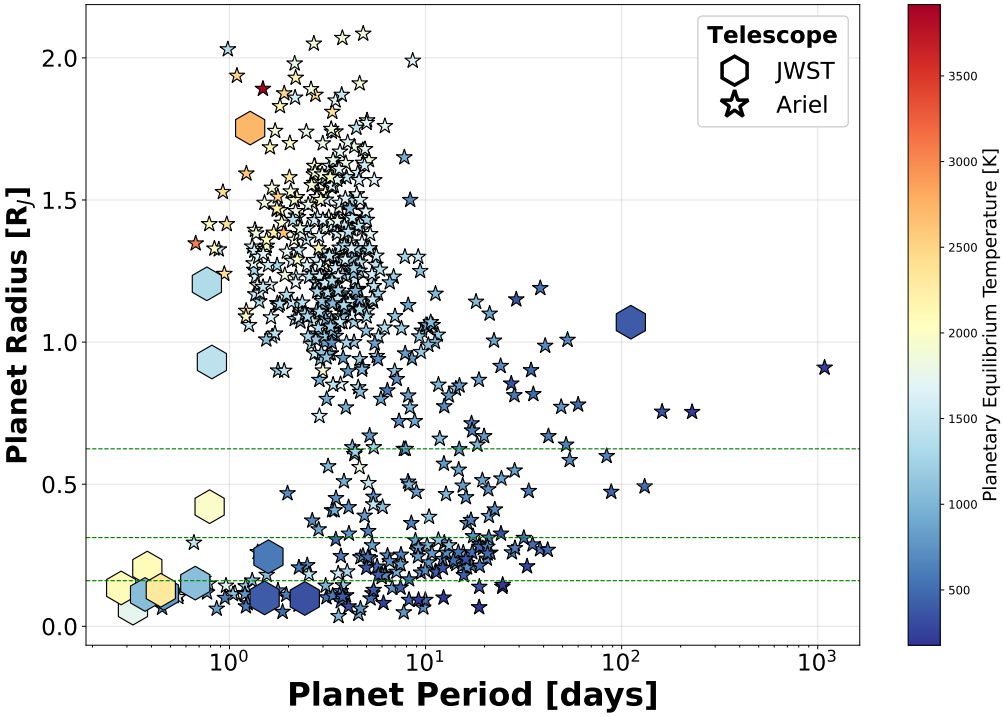

Figure 2: A comparison between JWST cycle 1 & 2 phase curve targets with the 605 Ariel potential targets selected by Edwards et al. [2019]. The horizontal green dashed lines correspond to the radius dividing rocky planest, sub-neptune, Neptunes, and gas giants. In all radius categories, current JWST proposals are aimed at the lowest-hanging targets with the shortest orbital period except HD 80606 b.

2 Methodology

2.1 Emission Spectroscopy Metric (ESM)

As a starting point, we compute the emission spectroscopy metric (ESM), a metric of evaluation originally for JWST targets, for all Ariel planets. The ESM gives a good approximation of the ex-

pected signal-to-noise ratio (S/N) for secondary eclipses detection in the mid-infrared and presents a general ranking of all Ariel targets for emission spectroscopy. Following Kempton et al. [2018], the ESM metric is defined as:

$$\mathrm{ESM} = 4.29 \times 10^6 \times \frac{B_{7.5}(T_{day})}{B_{7.5}(T_\star)} \times \left(\frac{R_p}{R_\star}\right)^2 \times 10^{-m_k/5}\,, \tag{1}$$

where T_{day} is the planet's dayside equilibrium temperature, which we take as $1.10 \times T_{eq}$ with T_{eq} as the planetary equilibrium temperature:

$$T_{\mathrm{eq}} = \left(\frac{1}{4}\right)^{1/4} T_\star \left(\frac{R_\star}{a}\right)^{1/2}\,, \tag{2}$$

where $T_\star$ is the stellar effective temperature and a is the semimajor axis. The radii of the star and the planet are $R_\star$ and R_p, m_k is the apparent magnitude of the host star in the K band, $B_{7.5}$ is the Planck function evaluated for a given temperature at a representative wavelength of 7.5 µm. Figure 3 plotted the 605 Ariel potential targets listed in Edwards et al. [2019] to illustrate their distribution over orbital periods and equilibrium temperature, with ESM color-coded. Both the planet and the star are assumed to be blackbodies. Although the assumption that a planet behaves as a blackbody in mid-infrared spectra is more arguable due to their strong molecular absorption and low opacity, it remains a reasonable assumption for characterizing the *relative* broadband observability of a planet [Kempton et al., 2018].

Edwards et al. [2019] uses another metric of evaluation for the 605 Ariel targets he selected, which is the number of required observations to reach each Tier's targeted Signal-to-Noise Ratio (S/N > 7) for transit and eclipses respectively. The smaller the required observations, the better the target. Here, we compare the ESM of Ariel targets and the required observations to observe Tier 3 Eclipses in Figure 4. The linear trend shown in this scattered plot indicated that both metrics equally evaluate the ranked signal strength of the targets.

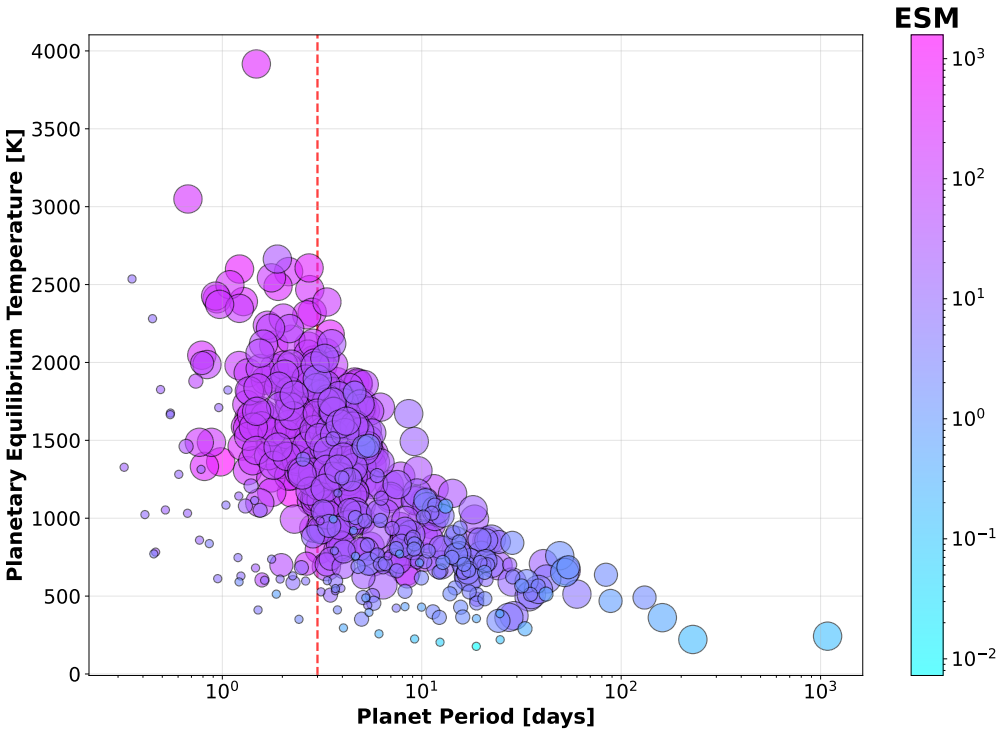

Figure 3: Temperature vs orbital period with Emission Spectroscopy Metric (ESM) as the color label for 605 Ariel targets from Edwards et al. [2019]. The horizontal red-dashed line indicates a period of two days. All targets are plotted with circles of different radii in ascending order to represent: terrestrial planets, sub-neptune, Neptunes, and gas giants. The targets with highest ESM (most purple) and shortest orbital period and generally all gas giants.

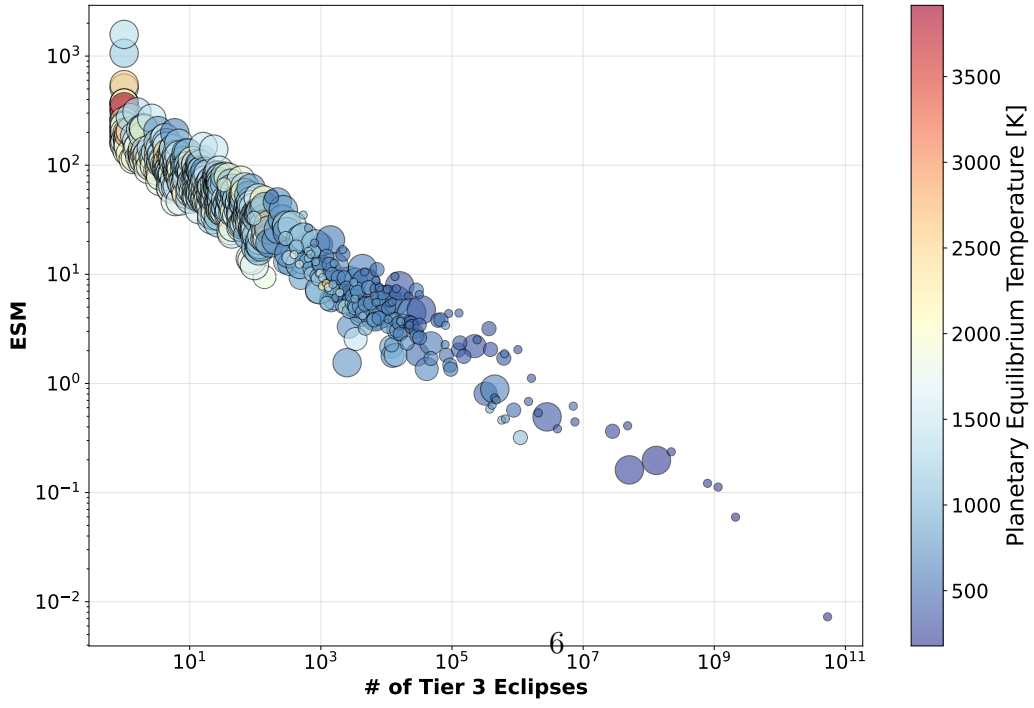

2.2 Ariel Target: Figure of Merit

In section 2.1 we have briefly evaluated all potential Ariel targets using metrics from other literature. Here, we define our own Ariel Figure of Merit (FoM) to rank and select targets for transmission and emission spectroscopy respectively. We will use this metric to evaluate the targets most suitable for phase curve and compare the results to Edwards et al. [2019] and Charnay et al. [2021].

2.2.1 Ariel Transmission Spectroscopy Metric (ATSM)

We begin by developing a metric for transit spectroscopy, termed the Ariel Transmission Spectroscopy Metric (ATSM). The amplitude of the transit spectral feature is expressed by the following [Cowan et al., 2015] :

$$A = 2R_{\rm p}N_{\rm H}H/R_\star^2\,, \tag{3}$$

where $N_{\rm H} = 5$ is the number of scale heights probed for targets in infrared [Tinetti et al., 2013, Mugnai et al., 2021]. The atmospheric scale height is expressed as $H = k_B T/\mu g$, with atmospheric temperature T, planet gravity g, and mean molecular weight μ. The atmospheric temperature is set to be T_{eq}. For each planet, we can compute a single amplitude across its entire observational wavelength.

2.2.2 Ariel Emission Spectroscopy Metric (AESM)

We also establish an emission metric for Ariel's target to assess both eclipses and phase curve spectroscopy observation called the Ariel Emission Spectroscopy Metric (AESM). We treat the planet and its host star as blackbodies, and thus the thermal contrast ratio can be modeled as [Cowan et al., 2015]:

$$[F_{\rm p}/F_\star]_{\rm therm} = (R_{\rm p}/R_\star)^2 B(\lambda, T_{\rm d})/B(\lambda, T_\star)\,, \tag{4}$$

where B is the Planck function given by:

$$B_\lambda(T) = \frac{2hc^2}{\lambda^5 e^{hc/\lambda kT} - 1}\,. \tag{5}$$

We take λ to range between 1.1 to 7.8 μm, and plot Equation (4) as a function of wavelength for each target. Figure 5 shows an illustration of four example targets in Ariel list (HIP 65 A(blue), WASP-178 (red), HAT-P-41 (green), and MASCARA-4 (orange)). The thermal contrast improves at longer wavelengths, asymptoting to the Rayleigh-Jeans limit of $(R_p/R_\star)^2(T_d/T_\star)$ when λ reaches infinity. In comparison to the ESM defined in section 2.1, which only evaluates the emission at $7.5\mu m$, this approach provides a comprehensive assessment of the thermal signal across the entire infrared spectrum.

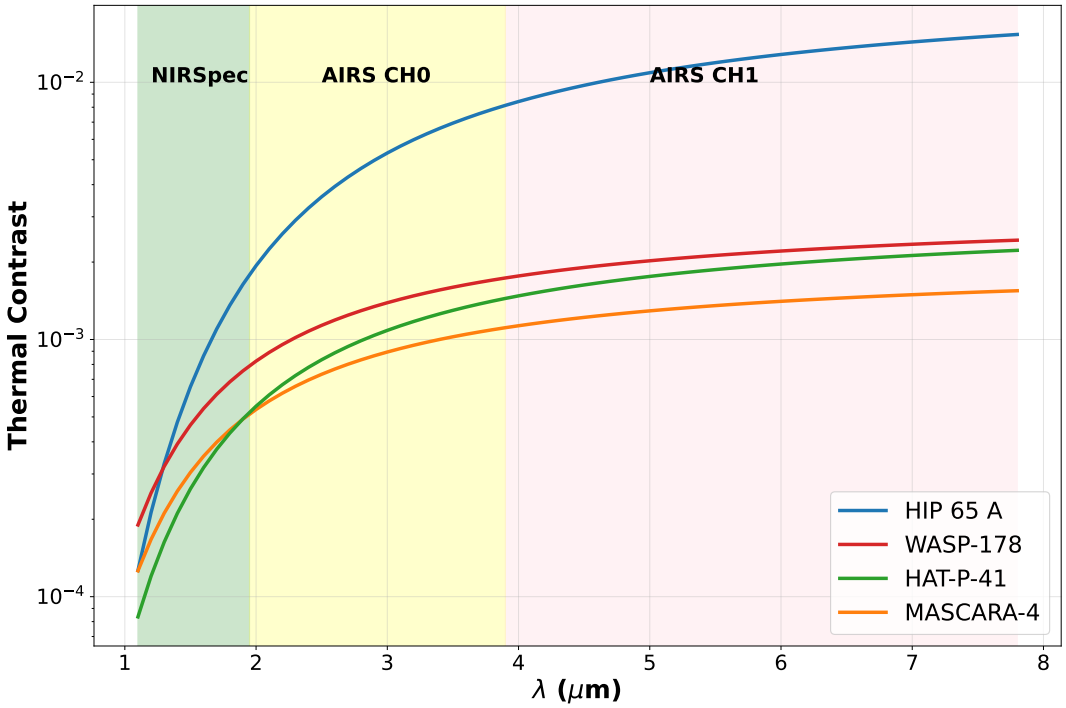

Figure 5: The thermal emission contrast of four example targets: HIP 65 A (blue), WASP-178 (red), HAT-P-41 (green), and MASCARA-4 (orange) as a function of wavelength. The green, yellow, and pink background indicate the operation wavelength for NIRSpec, AIRS-CH0, and AIRS-CH1 respectively. The thermal contrast improves at longer wavelengths and converges to Rayleigh-Jeans limit.

2.2.3 Photon-Couting Precision

The noise and precision of the target observed depend on the stellar parameters, its distance, the telescope diameters, as well as limited bandpass and imperfect system throughput [Cowan et al., 2015]. Hence the number of photons collected by an instrument within a time interval of Δt is:

$$N_{\rm phot} = \frac{\pi^2 \tau \Delta t}{hc} \left(\frac{R_\star D}{2d}\right)^2 \int_{\lambda_1}^{\lambda_2} B(\lambda, T) \lambda d\lambda \,, \tag{6}$$

where λ_2 and λ_1 are the limiting wavelengths of each bin, d is the distance to the star, $D = 1$ m is the telescope diameter, τ is the system throughput which we use 0.3 for NIRSpec and 0.2 for AIRS-CH0 and AIRS-CH1 [Tinetti et al., 2021], and Δt is the integration time, which we set as the transit duration for each target (for targets with circular orbit, the transit and eclipse duration are equal). In the Poisson limit for large number of photons, the precision is $\sqrt{\mathbf{2/N_{phot}}}$, where the factor of $\sqrt{2}$ accounts for a differential measurement with equal baseline outside of transit or eclipse.

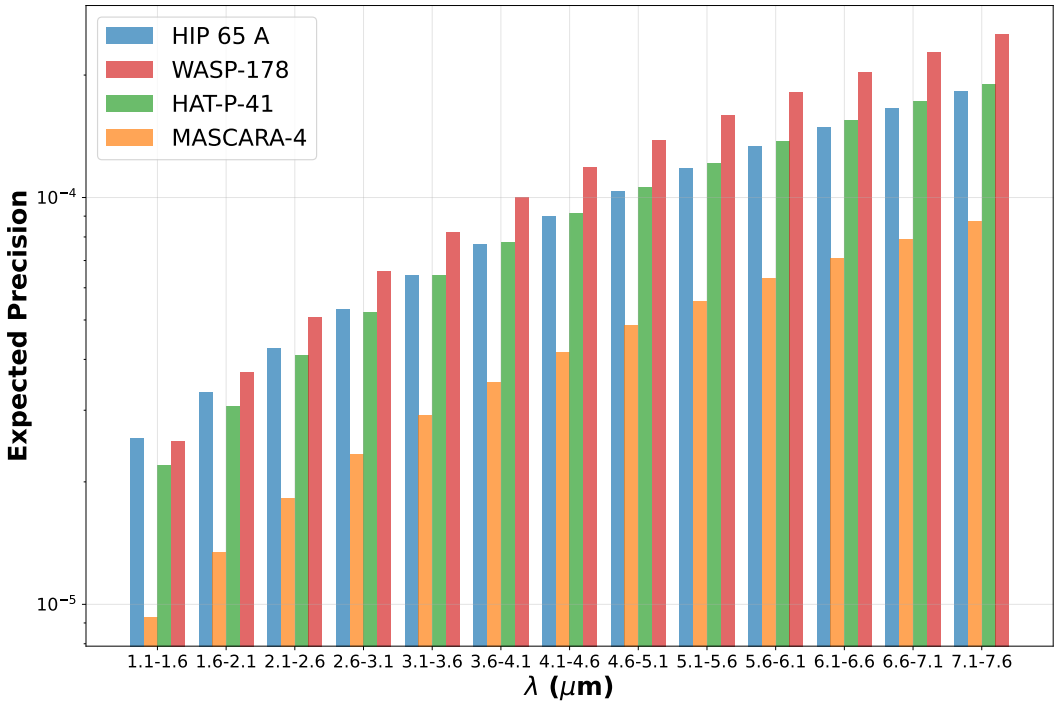

Figure 6: The expected photon-limited precision of the host star of four example targets: HIP 65 A (blue), WASP-178 (red), HAT-P-41 (green), and MASCARA-4 (orange) as a function of wavelength. Here, we binned the wavelength into 0.5 μm intervals as an example. The observing precision decreases at longer wavelengths as fewer stellar photons are available.

As an example, we calculate the expected precision of the host star for the same four sample targets as described in section 2.2.2, with wavelengths binned into 0.5μm each in Figure 6. The

expected precision worsens as we go to longer wavelengths as fewer stellar photons are available.

2.2.4 Figure of Merit (FoM)

For each target, we compute a Figure of Merit (FoM) for each Tier's transmission and emission spectroscopy to indicate its observability for a single inspection, also known as ATSM and AESM. To calculate the AESM, we first take the average thermal contrast in accordance with each photon precision bin. Then, each averaged thermal contrast is divided by its corresponding photon-counting precision, as shown in Figure 7. The final AESM is taken to be the average signal-to-noise (S/N) across all wavelength bins:

$$\mathrm{AESM} = \frac{\sum_i^{N_\lambda} F_i'/P_i}{N_\lambda}\,, \tag{7}$$

where F_i' is the thermal emission contrast and P_i is the photon-limiting precision in each N_λ number of bins. Similarly, ATSM is calculated by taking the ratio between transit spectra amplitude and average photon precision across all bins:

$$\mathrm{ATSM} = \frac{A/\sum_i^{N_\lambda} P_i}{N_\lambda}\,, \tag{8}$$

where A is the amplitude of the transit spectral feature in Equation 3.

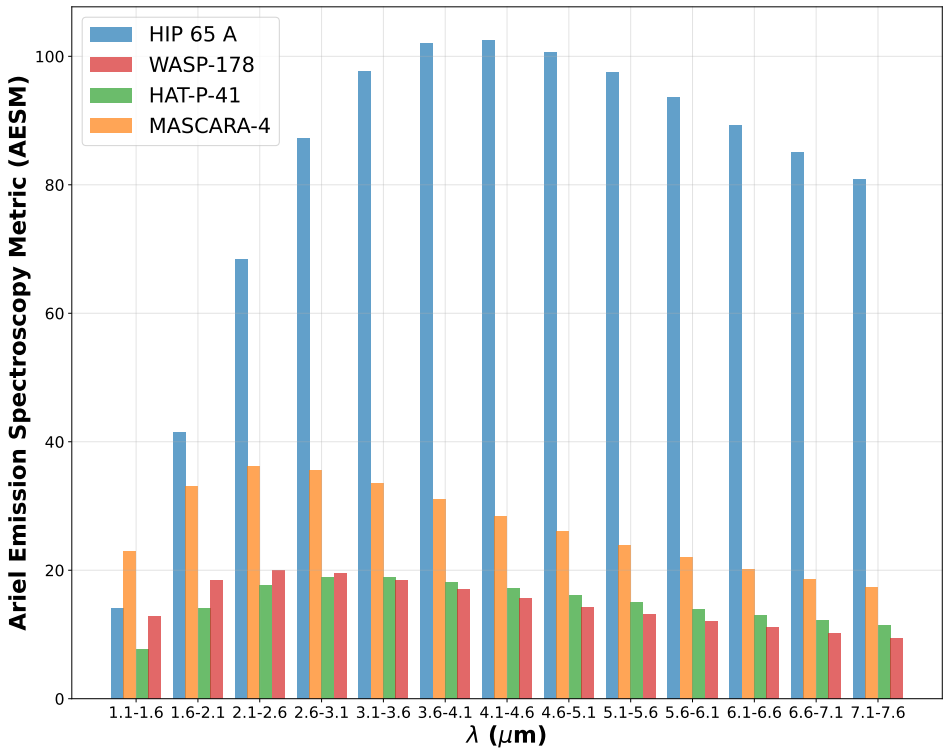

Figure 7: The Ariel Emission Spectroscopy Metric (AESM) of four example targets: HIP 65 A (blue), WASP-178 (red), HAT-P-41 (green), and MASCARA-4 (orange) in bins of $0.5\mu m$ in the wavelength of instrument NIRSpec, AIRS-0 and AIRS-1. The final FoM is calculated by taking the average across all bins to be 88.23, 24.00, 14.47, and 13.15v respectively.

By employing the aforementioned calculation schemes, we compute the FoM of all 605 Ariel targets from Edwards et al. [2019] for three tiers and for both transmission and emission spectroscopy. We divided the spectra into N_λ equally spaced bins across the three spectroscopy instruments: NIRSpec, AIRS-0, and AIRS-1, from wavelength 1.1 to 7.8 μm. Following Edwards et al. [2019], we select $N_\lambda = 5/75/150$ for Tier 1/2/3 respectively, as shown in Table 1. We are interested in calculating the number of targets reaching the observation threshold of 7. We also add in a comparison set with an observation threshold of 10 in Scenario 2.

	Scenario	S/N Threshold	N_λ (Tier 1/2/3)	λ Range (μm)
Edwards' Model	\	7	5/75/150	$1.1 - 7.8$
My Model	1	7	5/75/150	1.1 - 7.8
	2	10	5/75/150	

Table 1: Model parameter to calculate the Figure of Merit (FoM) for 605 Ariel targets from Edwards et al. [2019]. N_λ gives the number of equally spaced bins in the range of λ for each tier respectively. The first row listed out the original parameters used in Edwards et al. [2019] paper while Scenario 1 & 2 listed out the parameters and S/N threshold used in the model of this paper.

Scenario	ATSM			AESM		
	Tier 1	Tier 2	Tier 3	Tier 1	Tier 2	Tier 3
Edwards' Model	159	10	7	194	54	23
1	204	11	7	298	51	24
2	106	7	4	225	24	14

Table 2: Number of targets within the 605 exoplanets from Edwards et al. [2019] that reaches the S/N threshold for each Tier in Edwards' original model and the two scenarios in this model (see Table 1 for parameters). We see a close match of the number of observable targets between Edwards' Model and Scenario 1 for Tier 2 and Tier 3 targets in both transmission and emission spectroscopy.

As shown in Table 2, our results are consistent with the calculation of Edwards et al. [2019] for Tier 2 and Tier 3 targets. For Tier 1 results, we provide higher estimations for both transmission and emission spectroscopy. The discrepancy across Tier 1 results can be potentially due to different noise models. As detailed in ArielRad [Mugnai et al., 2020], a simulator of the Ariel radiometric model used by Edwards et al. [2019], Mugnai et al. [2021], it outputs a noise integrated over 1hr of observation time, while our model integrates over the entire transit/eclipse time directly.

In addition, we show the cumulative observational time required to observe all 605 targets from Edwards et al. [2019] to reach different tiers in emission spectroscopy (Figure 8a) and in transmission spectroscopy (Figure 8b). Those plots demonstrate the diminishing return on scientific output if we want to observe lower signal targets in higher resolution. For example, if given three years to complete phase curve inspection, we can observe 300 Tier 1 resolution targets, but only $\sim$ 120 Tier 2 resolution targets and $\sim$ 105 Tier 3 resolution targets. In order to maximize the

scientific return within Ariel's four-year mission lifetime, we should prioritize targets with higher signals to higher Tier observations, and survey the low-signal population with reduced resolution.

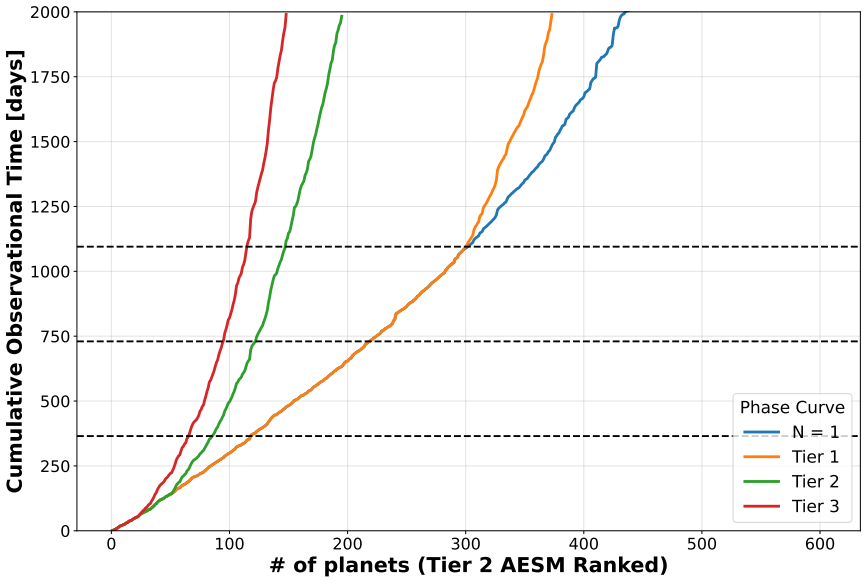

(a) The cumulative required observational time for each target to reach Tier 1 (orange), Tier 2 (green), and Tier 3 (red) resolution in Ariel Emission Spectroscopy Metric (AESM) for phase curves.

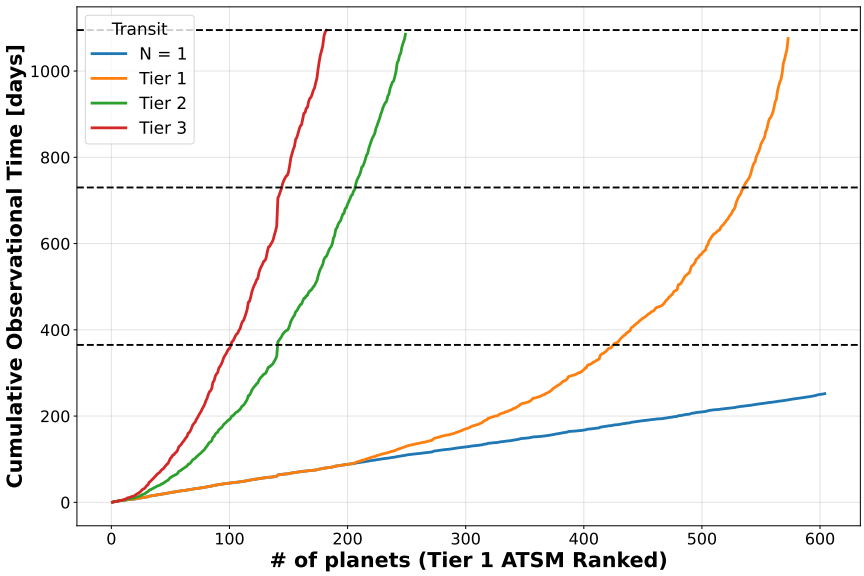

(b) The cumulative required observational time for each target to reach Tier 1 (orange), Tier 2 (green), and Tier 3 (red) resolution in Ariel Transmission Spectroscopy Metric (ATSM) for transit targets.

Figure 8: All targets are based on the master list from Edwards et al. [2019] ranked in AESM (Top) and ATSM (bottom) respectively. Notably, achieving a heightened resolution for lower signal targets necessitates a substantially increased investment in observation time. The $N = 1$ (blue) gives a reference observational time when all targets are only observed once. The horizontal dashed black lines represent one/two/three years of time.

2.3 Partial Phase Curve

Observing the full phase curve of all interested targets can be challenging due to limited telescope time. In those situations, one strategy is to observe only a partial phase curve for targets with orbital periods longer than 48 hours. Partial phase curves observations that start and end at an angle $45° < \theta < 90°$ before and after the eclipse are illustrated in Figure 9. The angle of the partial phase curve needs to at least cover the phase curve offset due to heat transport. Phase curve offset is the longitudinal separation between the substellar point and the peak of the phase curve [Penn and Vallis, 2018]. Based on the analysis presented in Figure 5 of Bell et al. [2021], which investigates the phase curve offset of 16 Spitzer 4.5 μm targets, we have chosen to employ a minimum angle of $\pm 45°$ in our selection.

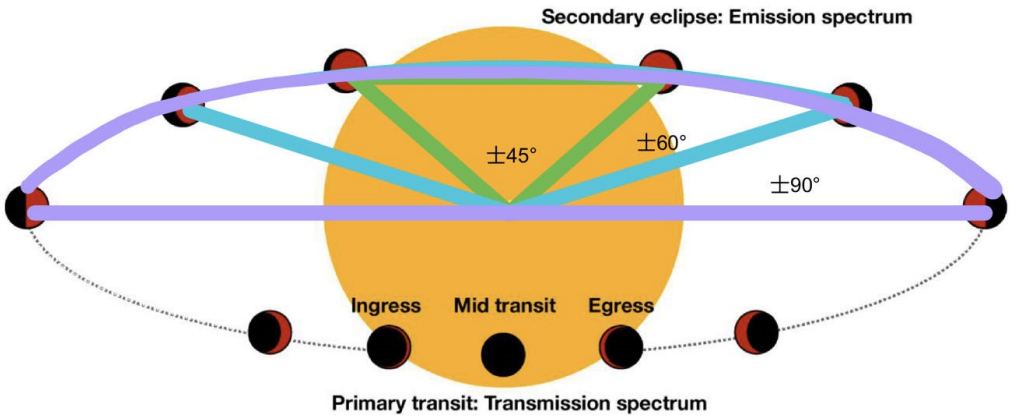

Figure 9: Transiting scheme of the partial phase curves observation of an exoplanet around its host star with angle $\pm 45°, 60°, 90°$ (green, blue, purple) before and after the eclipse to include at least the phase curve offset due to heat transport. Picture not to scale and adapted from Figure 2 of Pluriel [2023], an example phase curve of the hot Jupiter HD 189733 b observed at 4.5 microns with IRAC/Spitzer.

We first rank all 605 potential Ariel targets from Edwards et al. [2019] based on the values of Tier 2 AESM. All targets with an orbital period of more than 48 hours are observed only partially based on the observing angle θ selected. We proceed to calculate the number of targets that can be characterized within a 365-day period by cumulatively adding up all the observing periods (including two eclipses) in the order of ranking, as shown in Figure 10. *If Ariel would dedicate a full year to phase curve observation, with a $\pm 45°$ selected for partial phase curve, 61 full phase curve targets can be observed in addition to 215 partial phase curve targets.* Additionally, Figure

11 shows how those 276 Ariel targets compared with the known observations with Spitzer, Hubble, and JWST. In comparison to other targets, Ariel full phase curve clustered within 1 to 2 days, as opposed to < 1 day for JWST targets or up to 5 days for Spitzer targets. The partial phase curve of Ariel spans a wider parameter space with an orbital period over ~ 10 days and exoplanets with extremely low gravity.

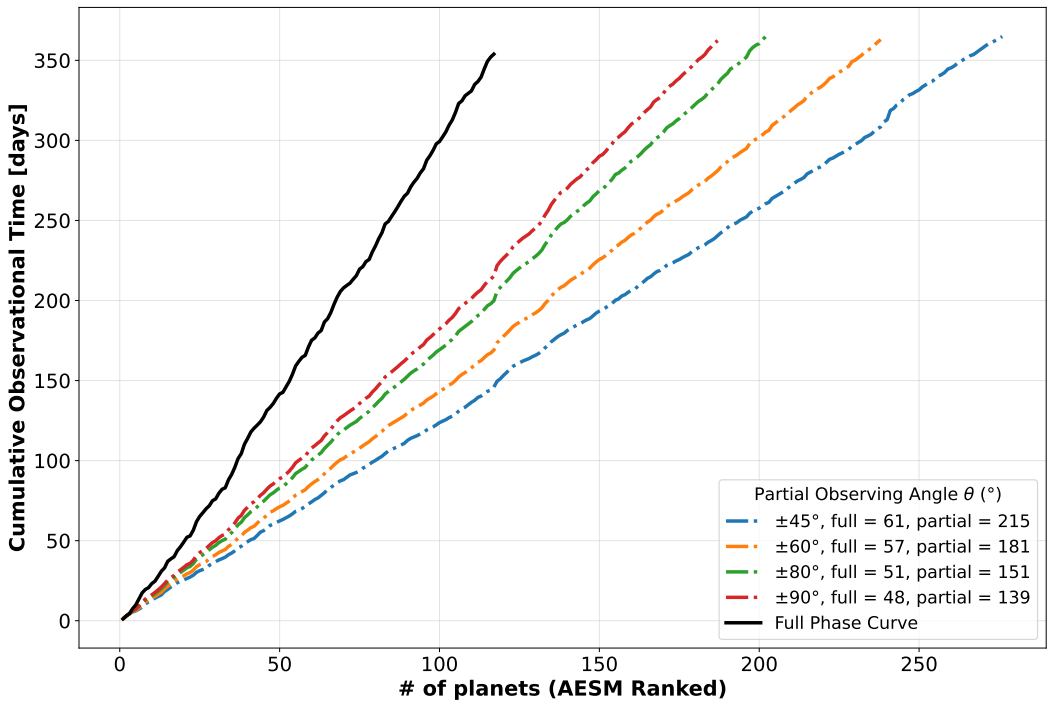

Figure 10: The number of targets that are observable given 365 days for different partial phase angle ($\pm\theta$) observation. The potential 605 Ariel targets from Edwards et al. [2019] are ranked based on Tier 2 AESM. All exoplanets with orbital period ($P_{\rm orb}$) longer than 48 hours are observed with partially: $\frac{2\theta}{360^\circ}P_{\rm orb}$. The cumulative time then adds the final period in the order of ranking. The lower right legend shows the number of planets that can be observed with full and partial phase curves given 365 days.

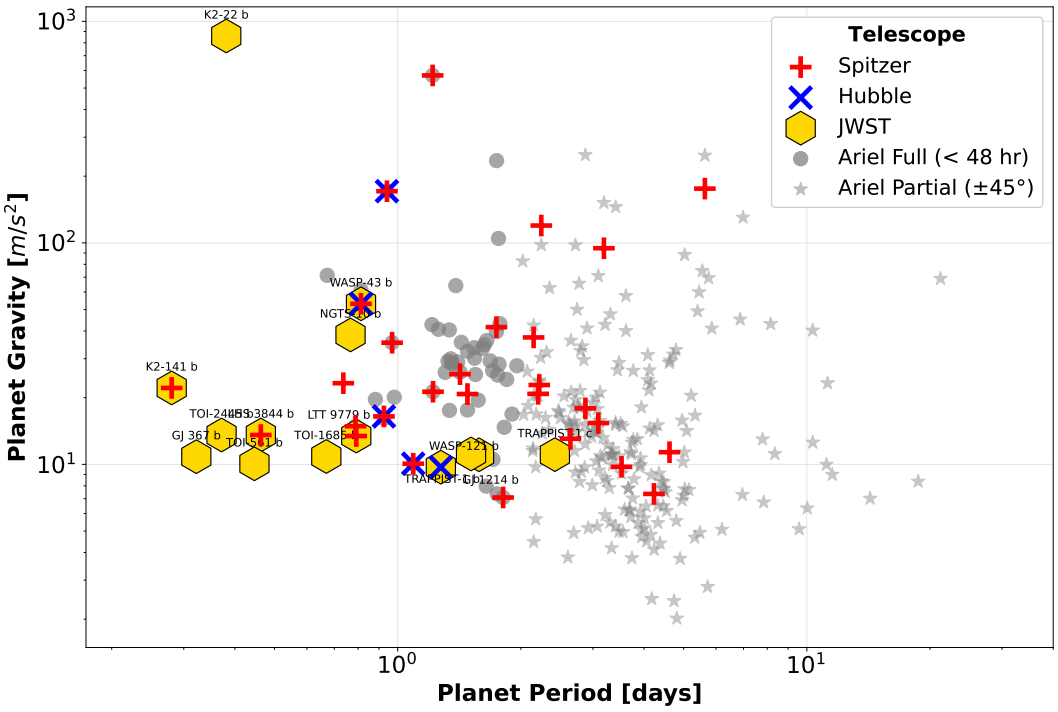

Figure 11: Spitzer, Hubble, JWST cycle 1 & 2, and Ariel targets for phase curve. The selected ariel targets are those under a cumulative observing time of 365 days following the ranking of Figure 10. Most JWST targets orbit with a period of less than 2 days and have a gravity of at least 1 g. In comparison, Ariel targets, both full (52) and partial (207), cover a wider range of the parameter space.

3 Phase Curve Target List

Target selection for transit and eclipses was done by Edwards et al. [2019] with an emphasis on satisfying the scientific goal of chemical fingerprint and elemental composition. In comparison, phase curve target selection requires more planning as it demands long periods of continuous observation, even up to tens of days. Charnay et al. [2021]'s study proposed an observation strategy to select targets based on classes of planet radius (detailed in section 3.1). This method, even though covering a wide range of planetary radii with short periods, might require a substantial amount of follow-up observation due to their low visibilities. Here, we proposed another selection method by ranking all targets based on their Ariel Emission Spectroscopy Metric (AESM) as described in section 3.2.

3.1 Best in Class Method

The Ariel Consortium usually requires the target selected for Ariel to be even across different classes based on characteristics such as radius or temperature to ensure heterogeneity. A previous Ariel phase curve target list study by Charnay et al. [2021] recommended a selection criteria based on planetary radius:

1. rocky planets with planetary radius $R_p < 0.16R_J$
2. sub-Neptunes with planetary radius $0.16R_J < R_p < 0.312R_J$
3. Neptunes with planetary radius $0.312R_J < R_p < 0.624R_J$
4. Gas giants with planetary radius $R_p > 0.624R_J$

In each class, they select targets with $S/N > 10$ in Tier 1 photometric phase curve and select gas giants with $S/N > 10$ in Tier 2 for the emission spectroscopy. They found that 44 ideal planets with periods less than 5 days can be observed within $\sim 10\%$ of Ariel's science time, not considering re-observation.

Using a similar strategy, we select the six targets with the highest Tier 2 AESM in each class of terrestrial, Neptune, and sub-neptune planets. For gas giants, we select the top 25 targets with Tier 2 AESM > 7, giving us a total of 43 targets, listed in Appendix A. This target selection method allows us to cover planet phase curves of a wide range of planet gravity and orbital periods to ensure a diverse and complete target list (Figure 12). The cumulative observational time needed for those targets is 115.57 days (8% of total mission lifetime) for full phase curve observations, as shown in Figure 13a. If we employ partial phase curve observations for targets that orbit longer than 2 days, $\sim$ 75 days are needed for $\pm 90^\circ$ observations, and $\sim$ 55 days are needed for $\pm 45^\circ$ observations. Among those, the overlapping time for transit observations is $\sim$ 15.4 days if observing full phase curves, which reduces the time dedicated to phase-curve to 6.8%.

However, the signal from most rocky, sub-Neptune, and Neptune planets does not reach Tier 2 AESM requirement, and multi-epoch observations are needed to yield a good scientific return.

Since the increase in S/N is proportional to the square root of observation duration, we calculate the integer number of observations needed to reach Tier 2 AESM for each target:

$$N_{\rm obs} = \lceil 7/{\rm AESM}_2 \rceil \, , {\rm AESM}_2 < 7 \, . \tag{9}$$

Using our new $N_{\rm obs}$, the total cumulative time to observe those targets increases to 5283 days for full phase curve observations, as shown in Figure 13b. If we choose to observe a $\pm 45^\circ$ for partial phase curve, within a 365-day mission timeframe, we can observe only 31 targets (25 gas giants, 4 Neptunes, and 2 sub-Neptunes). The turning point of the plot begins when all gas giants are observed, and the subsequent targets requires high numbers of re-observation to reach desired resolutions. The scientific return of observing only 31 targets using a full year of mission lifetime is too low. Allocating significant resources of the Ariel mission towards these low-signal targets seems unjustified, especially when considering the potential compromise on the total count of observable targets.

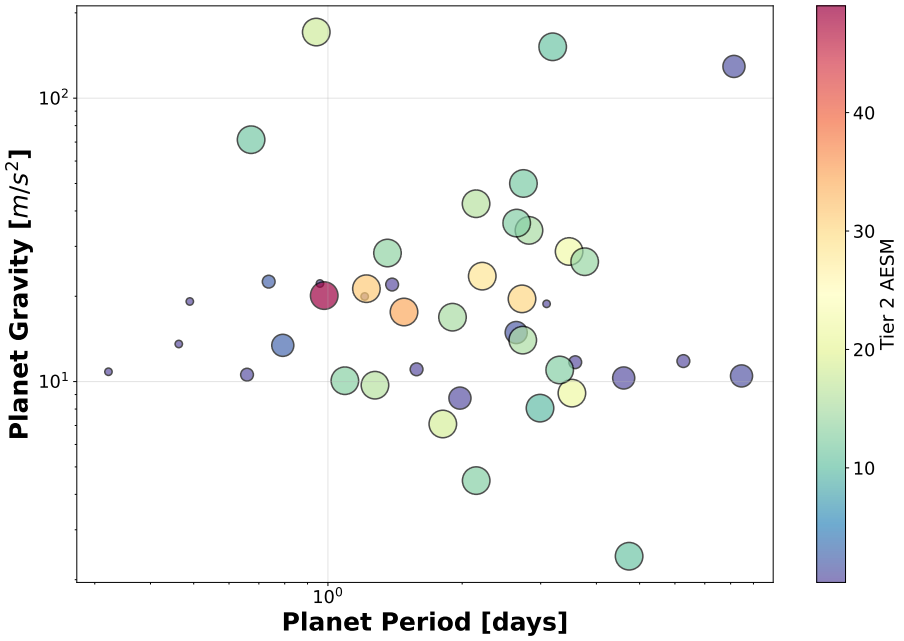

(a) 43 targets selected via Best in Class Method are plotted with circles of radii in ascending order to represent: terrestrial planets, sub-neptune, Neptunes, and gas giants. Most rocky, sub-Neptune, and Neptunes do not reach Tier 2 AESM requirements and potentially need re-observations.

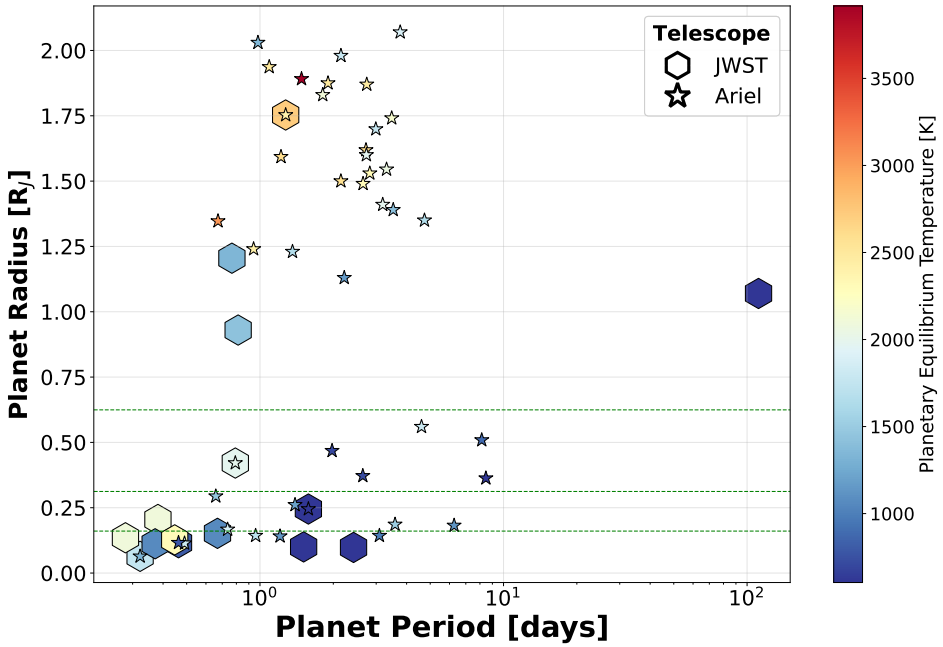

(b) Comparison of the 43 selected targets with JWST cycle 1 & 2 phase curve targets. Five of the targets overlap with the current JWST phase curve selections.

Figure 12: 43 targets selected based on the Best in Class method (i.e. to include planets in all radius range) from the 605 listed in Edwards et al. [2019]. The top 6 emission targets are selected from each class: rocky, Neptune, and sub-neptune planets and the best 25 AESM targets are selected for gas giants.

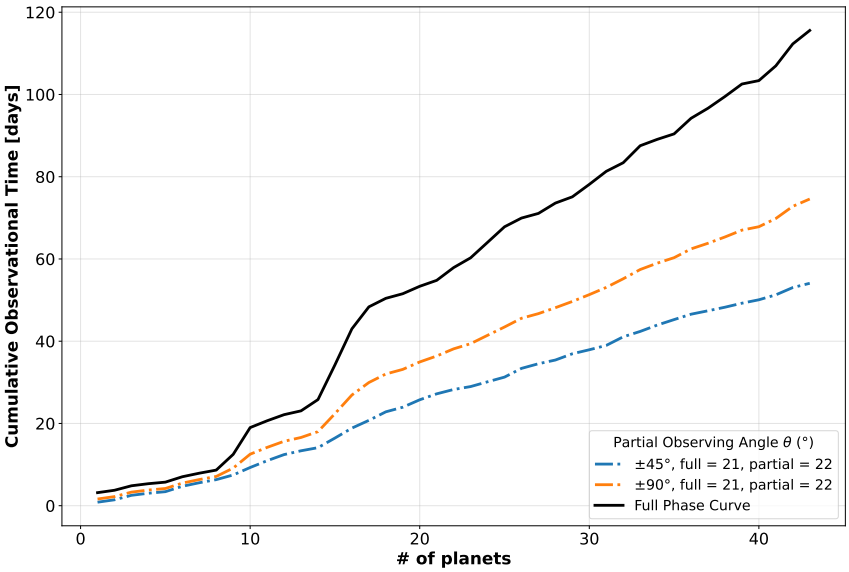

(a) The total observational time needed for the 43 targets selected based on Best in Class method when all targets are observed only once.

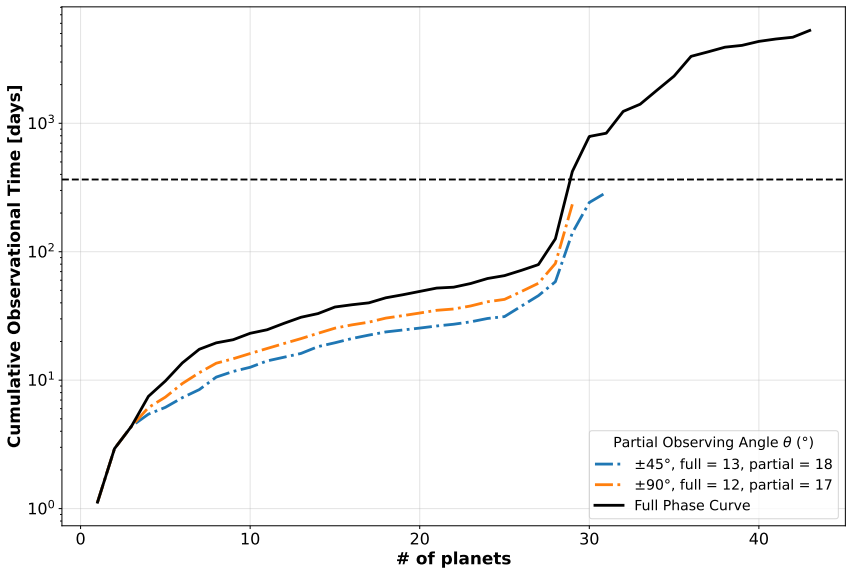

(b) The cumulative time needed to observe the 43 selected targets with Best in Class method if we reobserve all planets with $AESM < 7$ to reach Tier 2 resolution.

Figure 13: The cumulative time to observe the 43 targets selected via Best in Class (from a total of 605 targets [Edwards et al., 2019]) for two observational strategies. The blue and orange line shows the amount of observational time needed for partial phase curve observations of targets with orbital period > 48 hrs for $\pm 45°$ and $\pm 90°$ respectively. To complete full phase curve observations for all targets at a sufficiently high resolution, more than 5000 days of science time is required.

Additionally, we consider the scenario in which we have a full year dedicated to phase curve observation and require only one observation for each target using the Best in Class method. We choose to allocate the same amount of observational time to each class. Using this method, we can acquire 44 rocky planets, 14 sub-Neptunes, 16 Neptunes, and 34 gas giants for full phase curves observation. If we consider a partial phase curve observation with $\pm 45°$, we found 61 terrestrial planets, 34 sub-Neptunes, 36 Neptunes, and 51 gas giants to be observable within 365 days. Even though the total number of observed targets is high, the average Tier 2 AESM is as low as ~ 3.93, significantly below the resolution required for Tier 2 observations. Consequently, we propose an alternative target selection approach in the subsequent section to create a list with higher scientific returns within the same or less timeframe.

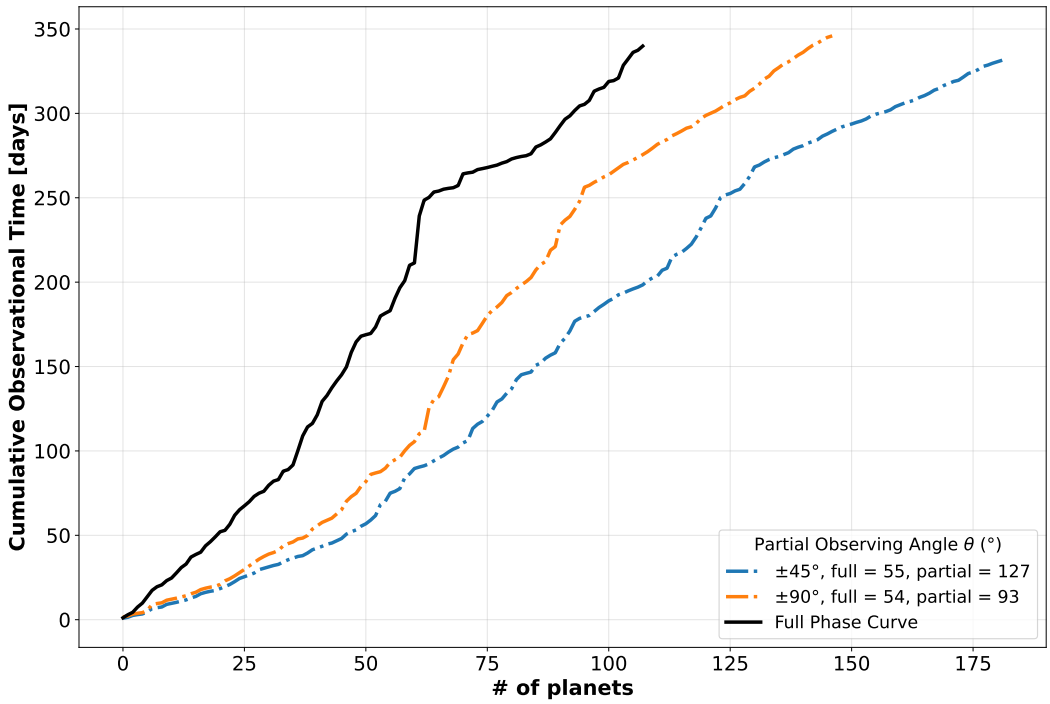

Figure 14: The total number of planets observable within a 365-day timeframe using the Best in Class (BIC) method when all targets are observed only once. Each class is allocated a quarter of the year of observational time. We can observe in total 108 full phase curves with 44 rocky planets, 14 sub-Neptunes, 16 Neptunes, and 34 gas giants with this method. However, the average Tier 2 AESM for all the targets is ~ 5.32, which is below the required resolution for Tier 2 observations.

3.2 Ranked FoM Method

In this section, we introduce another formalism for selecting phase curve targets based on their AESM (detailed in section 2.2.2). We rank all targets in descending order of AESM and select the first 51 targets, which have $AESM > 7$, as listed in Appendix B. The remaining targets serve as a backup observation plan if more observational time is granted. The distribution of planet gravity, period, AESM, and radius of those 51 targets are shown in Figure 15 and 16. In comparison to the Best in Class method, those targets are more clustered in short observational periods with higher signals. All planets are Jovian planets with an orbital period of less than 5.5 days. Notably, all 51 targets exhibit a high enough AESM so that each of them requires only a single observation to obtain reliable and accurate data.

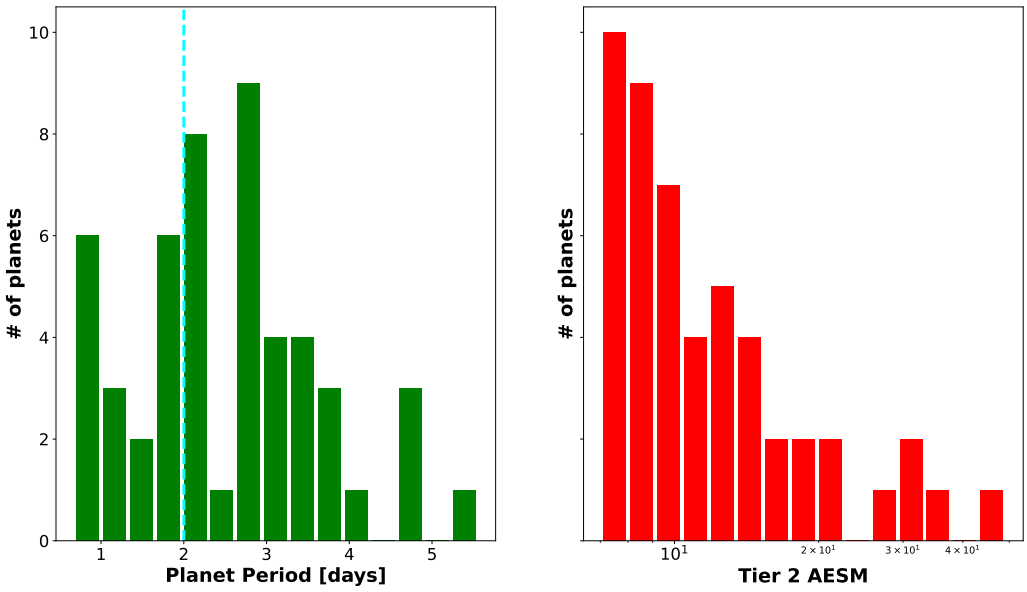

Figure 15: Histogram of the distribution of 51 targets selected based on Ranked FoM Method as a function of the orbital period (green) and Tier 2 AESM (red). The vertical dashed cyan line in the left plot indicates an orbital period of 2 days, which all planets beyond will be observed with partial phase curves. All planets but one lie within an orbital period of 5.5 days, and AESM > 7.

If we choose to observe full-phase curves of all those 51 targets, a total observational time of $\sim$ 140 days is required (including two eclipse observations, $\sim$ 10.42% of the total mission lifetime), as shown in Figure 17. If we employ partial phase curve observation for planets with orbital period

greater than 48 hours, we can acquire 17 full phase curves and 34 partial phase curves, significantly more than the 13 full and 18 partial phase curves in the Best in Class method. Additionally, a $\pm 45^\circ$ partial phase curve observation only requires $\sim$ 60 days, which is a reduced observational timeframe of **300** days from the previous method.

If we can allocate additional science time to phased curve observations, assuming up to 365 days (approximately 25% of the mission lifetime) and reobserving the backup targets until the desired resolution for planets with AESM < 7, we have the potential to observe 85 full phase curves (see Figure 18). If we adopt partial phase curve observations strategy, we can observe up to 36 full phase curves and 99 partial phase curves with $\pm 45^\circ$ (31 full and 80 partial for $\pm 90^\circ$). The distribution of those 135 targets (with partial phase curve of $\pm 45^\circ$) are shown in Figure 19 and 20. All of those planets remain Jovian planets with a period with Gaussian distribution centered on 3 days.

Additionally, we consider the case when all targets are only observed once within a timeframe of 365 days, regardless of their Tier 2 AESM. This is exactly the scenario in Figure 10. Within 365 days, we can observe 61 full phase curves and 215 partial phase curves ($\pm 45^\circ$), with 274 of those being gas giants, 1 Neptune, 1 sub-Neptune, and 0 rocky planets. However, the average AESM is around 5.37 for those targets, which is below the required threshold for Tier 2 emission spectroscopy.

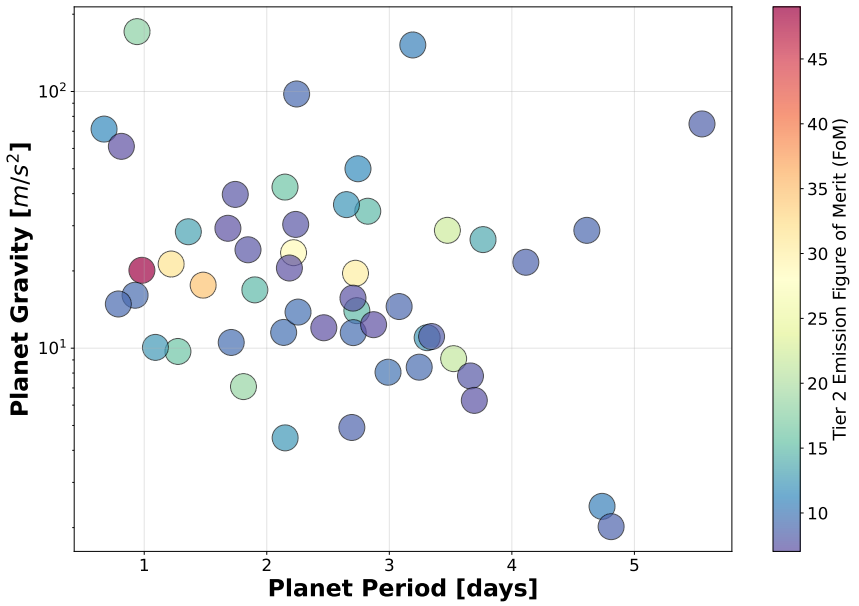

(a) The gravity and orbital period of 51 targets reaching Tier 2 AESM. Most targets have an orbital period of less than 5 days with a wide range of planet gravity. All targets have at least an AESM of 7 with the highest reaching ~ 50.

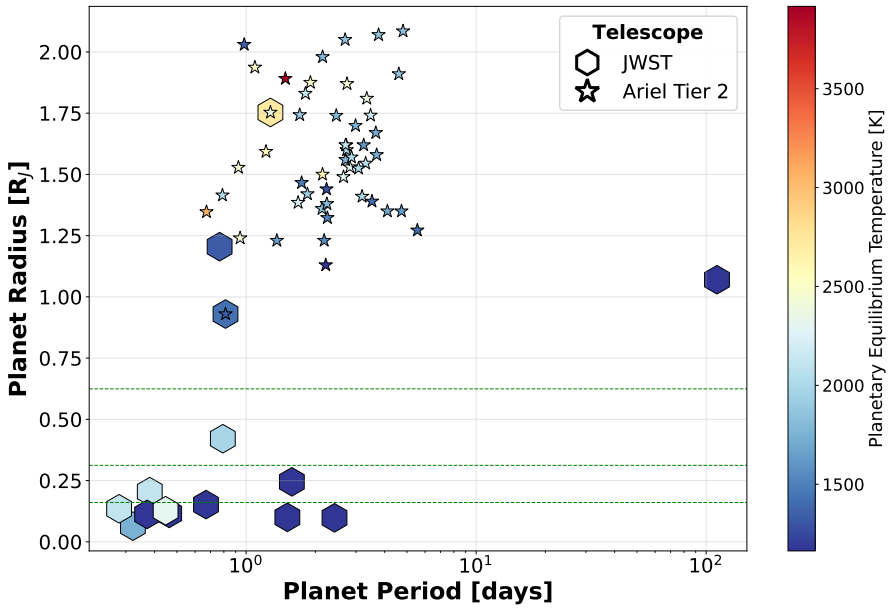

(b) Comparsion of JWST cycle 1 & 2 phase curve targets with Ariel selection (51 targets reaching Tier 2 AESM) as a function of radius and orbital period. All targets are gas giants with orbital periods between 0.9 – 9 days and $R_J > 0.93$. Two of the targets overlap with previous JWST phase curve observations.

Figure 16: 51 targets reaching Tier 2 Ariel Emission Spectroscopy Metric (AESM) selected from the 605 targets from Edwards et al. [2019]. All selected targets are Jovian planets as they have the highest scientific return in thermal emission spectroscopy.

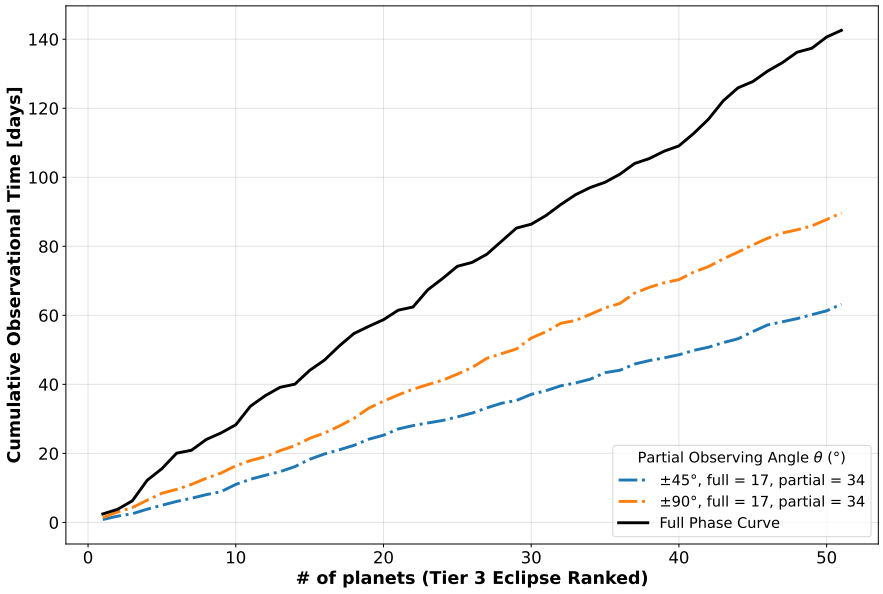

Figure 17: The cumulative observing time for the 51 Tier 2 targets with AESM > 7. If all targets are observed with full phase curves, we need ~ 140 days, while with partial phase curves of $\pm 45°$ and $\pm 90°$, only ~ 60 days and 90 days are needed.

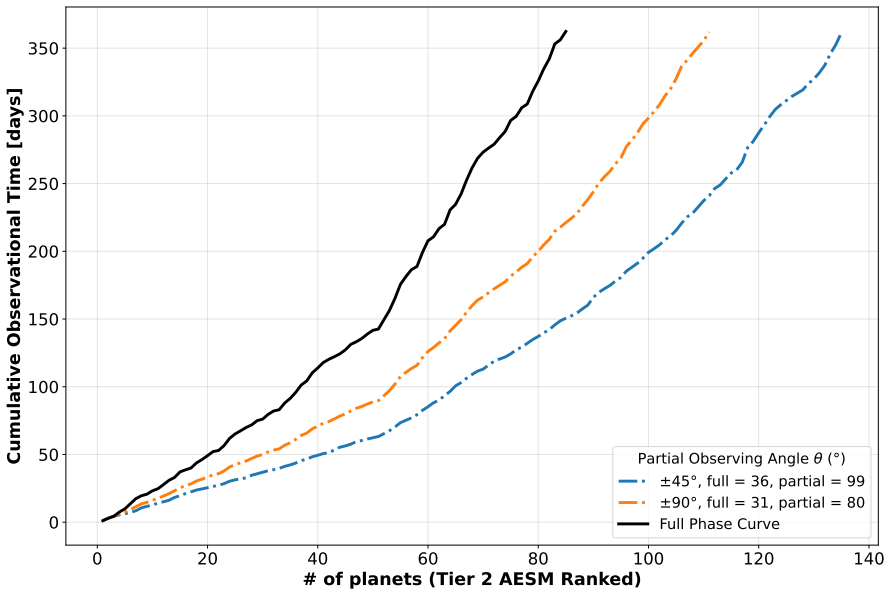

Figure 18: The number of targets observable when all targets are reobserved until Tier 2 resolution within 365 days of cumulative observations. We can observe a total of 85 full phase curve targets. With partial phase curve of $\pm 45°$, we can observe 36 full phase curves and 99 partial phase curves.

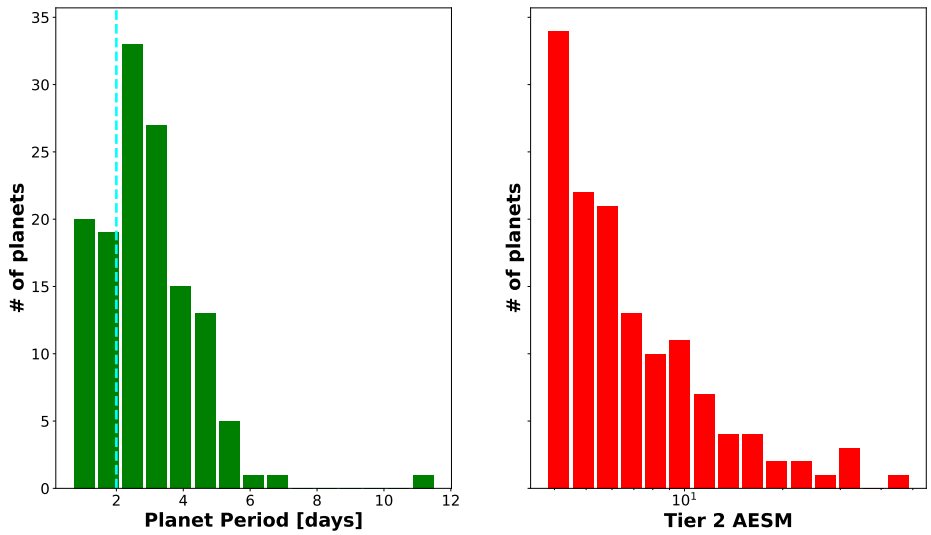

Figure 19: Histogram of the 135 targets selected based on Ranked FoM Method as a function of the orbital period (green) and Tier 2 AESM (red). All targets are reobserved to reach Tier 2 AESM. Those targets are selected to be within a cumulative period of 365 days and with a partial phase curve angle of ±45°. Most targets still cluster within an orbital period of 5 days and have at least a Tier 2 AESM > 3.78.

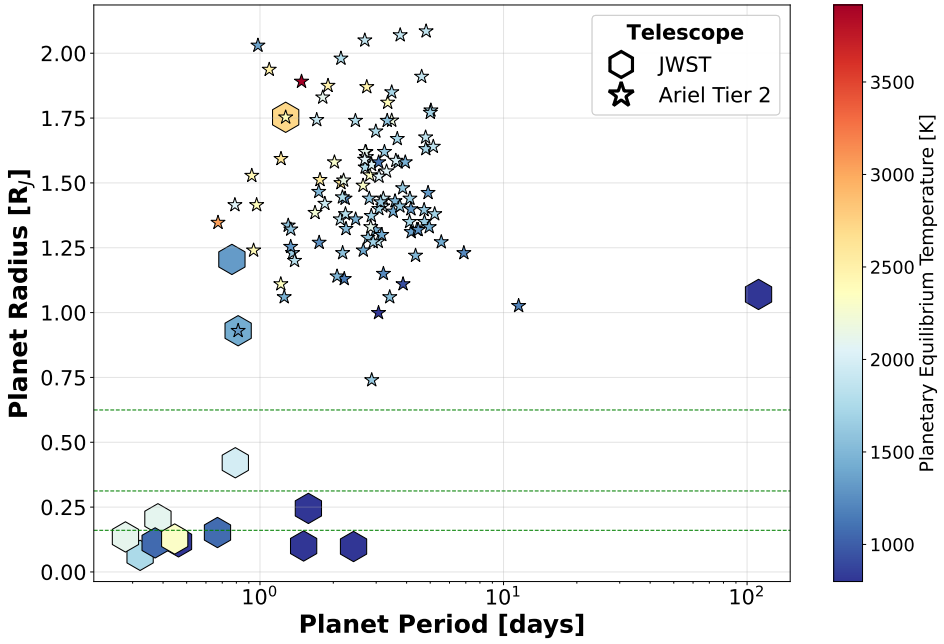

Figure 20: The distribution of radius and orbital period of 135 targets selected based on Ranked FoM Method within 365 days with partial phase curve observation of ±45°, re-observed until Tier 2 AESM resolution. All targets are gas giants with orbital periods less than 10 days and $R_J > 0.75$.

3.3 Comparing Different Phase Curve Targets

We show a comparison between the Best in Class (BIC) method and Ranked FoM Method (RFM) in Table 3 under two scenarios: when the targets are re-observed until Tier 2 AESM resolution, and when the targets are only observed once.

	Cumulative Observational Time [days]	Full Phase Curve	Partial Phase Curve ($\pm 45°$)	Gas Giant / Neptune / Sub-Neptune / Rocky	Average Observation Days	Average $N_{\rm obs}$	Average AESM
Best in Class (Tier 2 AESM)	365	13	18	25/4/2/0	1.46	6.38	15.21
Ranked FoM (Tier 2 AESM)	365	36	99	135/0/0/0	1.31	2.03	8.12
Best in Class ($N = 1$)	365	55	127	61/34/36/51	2.01	1	3.93
Ranked FoM ($N = 1$)	365	61	215	274/1/1/0	1.41	1	5.37

Table 3: Comparision of four methods for Ariel phase curve selection in a cumulative observational time fo 365 days. The first and third column requires the targets to be reobserved while Tier 2 AESM is met, while the second and fourth columns look at the case when only one observation is granted. In the same timeframe (Tier 2 AESM required), the Ranked FoM method can observe 23 more full phase curves and 81 more partial phase curves with an average number of observations 3 times lower. In the case of only one observation, the average AESM is well beyond the resolution threshold of 7.

In the Tier 2 AESM scenario, our results demonstrate that over a span of 365 days, the RFM approach allows the observation of 104 additional phase curves (comprising 23 full and 81 partial phase curves) compared to the BIC method. Furthermore, the RFM exhibits a lower average observational time and a lower average number of observations. Surprisingly, the average AESM of BIC is actually higher than that of the RFM even though it includes many low-signal rocky planets. This is because the RFM target list contains large number of planets that have AESM clustered around 4 - 7, as shown in Figure 21. While even though the BIC targets can be as low

as ~ 0.4 Tier 2 AESM, more data is distributed in the higher value regions and yields an average AESM around 15. We also show the number of targets observable by those two methods within a timeframe of 365 days in Figure 22. The required cumulative time to observe only 43 targets selected via BIC is one order of magnitude higher than the cumulative time to observe 85 targets selected using RFM.

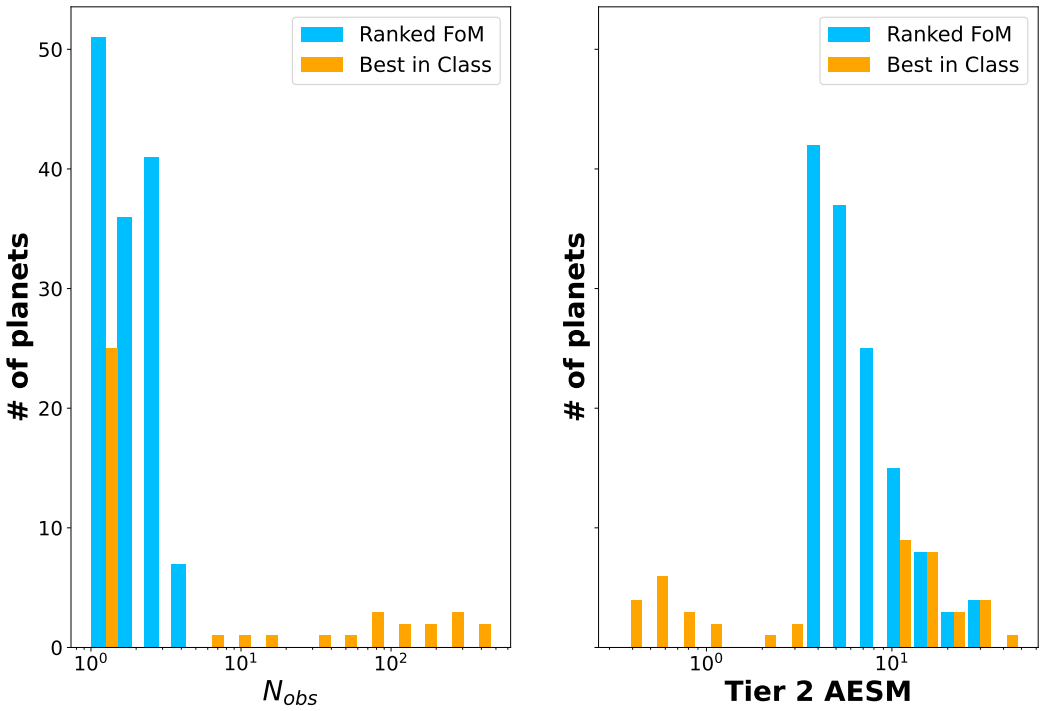

Figure 21: Histogram comparing the number of observations (left) and the Tier 2 AESM (right) of potential Ariel phase curve targets selected from two different methods: Ranked FoM Method (RFM) and Best in Class (BIC). All targets are re-observed until Tier 2 AESM is reached. The RFM targest have high numbers of targets clustered at low numbers of observations needed, while the BIC can have re-observations up to a few hundreds. The RFM targets have AESM clustered around 4 - 7, in contrast to BIC targets which can be as low as ~ 0.4.

In the scenario when we only observe all targets once, our results show that we can characterize 182 and 276 targets via the BIC and RFM methods respectively. Even though the BIC methods can observe targets with very short orbital periods, their Tier 2 AESM can be as low as $\sim 10^{-3}$, as shown in Figure 23. The targets selected via RFM have Tier 2 AESM clustered around 3 - 5. Even though observing each target once allows us to maximize the number of targets covered

by Ariel, the average signals are 3.93 and 5.37 for BIC and RFM respectively, which does not allow us to perform useful scientific analysis.

Regardless of the number of observations, the targets selected via the Ranked FoM method primarily focus on Jovian planets, as they showcase the most robust thermal emission spectroscopy. The deficiency of terrestrial and (sub) Neptune planet observations can be complemented with the JWST phase curve targets, which is designed to characterize small-radius rocky worlds, and is likely to complete dozens of observation before the launch of Ariel.

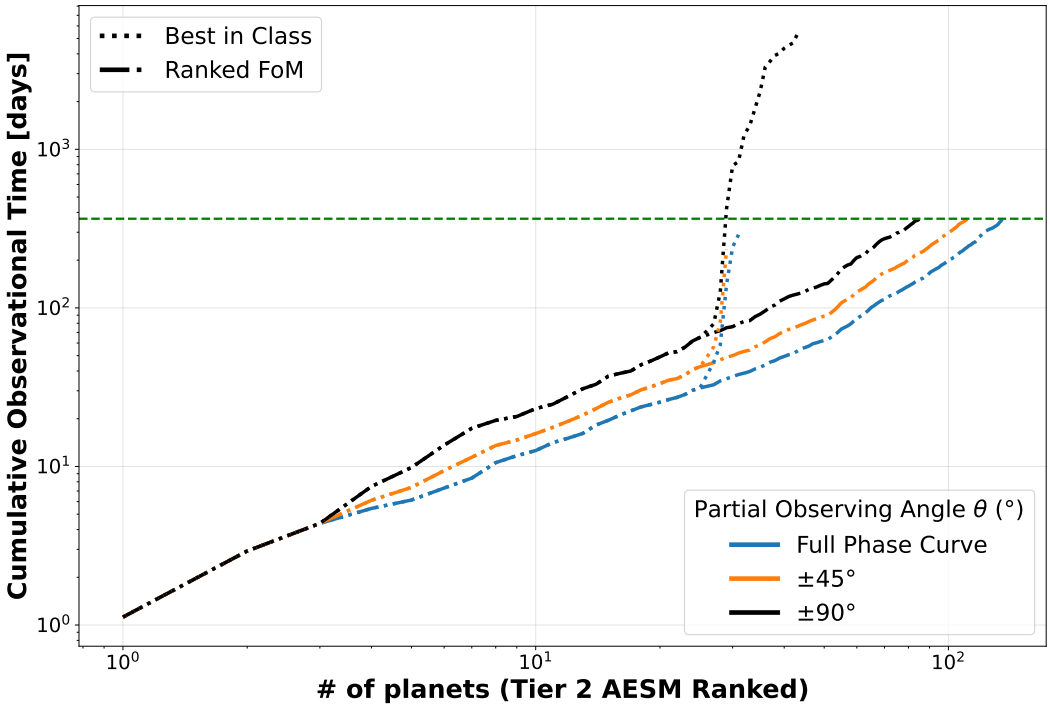

Figure 22: The number of targets observable given 365 days of cumulative observational time using two target selection strategies and three partial phase curve plans. The ranked FoM method is able to characterize 70 - 80 more targets in a given timeframe.

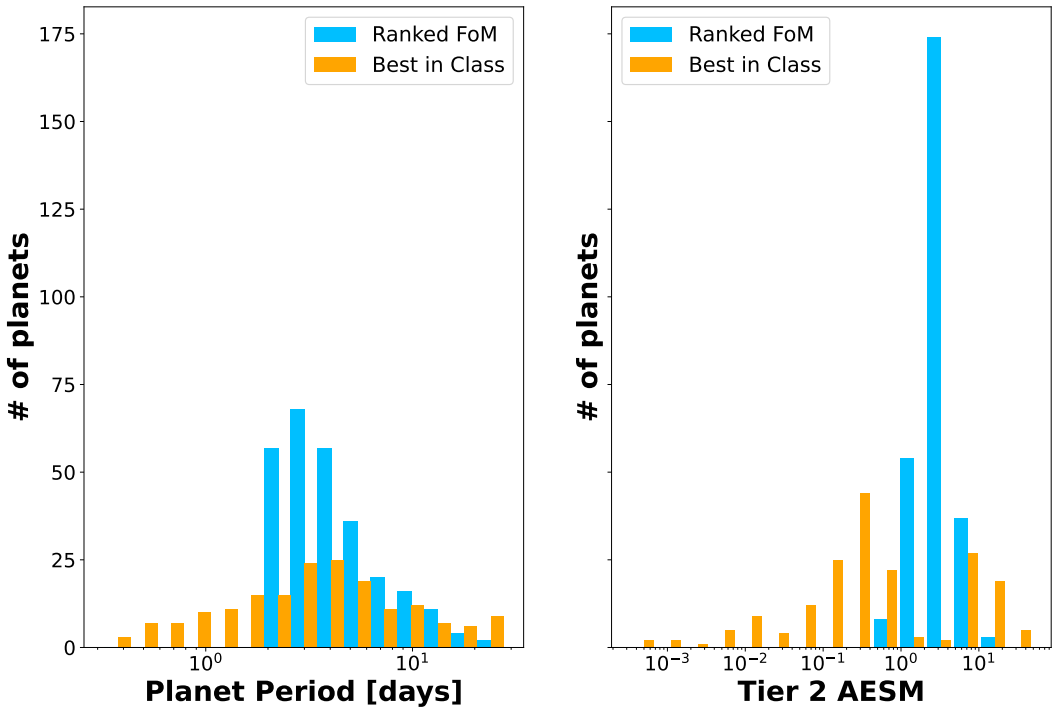

Figure 23: Histogram comparing the orbital period (left) and the Tier 2 AESM (right) of potential Ariel phase curve targets selected via two methods: Ranked FoM Method (RFM) and Best in Class (BIC). All targets are observed only once. The RFM targets are clustered between 2 - 5 orbital period and 3 - 5 AESM. The BIC targets, while some have short periods their AESM can drop to $\sim 10^{-3}$.

4 Transit Target List

4.1 Ranked FoM Method

Following the Ariel Transmission Spectroscopy Metric (ATSM, section 2.2.1), we design a preliminary transit target list based on their ranked ATSM. Given that the approach yielding the highest scientific return while optimizing time efficiency involves scheduling observations of the highest signal targets at higher resolutions (as illustrated in Figure 8b), we begin selecting the targets from Tier 3 down to Tier 1. By doing so, we aim to enhance the scientific return of these targets and optimize our observational strategy for the mission.

We begin by selecting Tier 3 targets with the top 60 planets with the highest ATSM, which

is roughly 10% of the initial target population we had. Within the rest of the potential targets, we select the ones that can be observed in 365 days as Tier 2 transmission targets. We then categorize the rest of the targets to Tier 1 observation, capping the total cumulative observation time at 3 years. This gives us 60 Tier 3 targets, 95 Tier 2 targets, and 369 Tier 1 targets (a total of 524 planets), as shown in Figure 24. We conveniently traced out the required observational time if we wanted to observe more/fewer transit targets in each tier using dashed lines. As indicated by the gradient of each tier, if we want to characterize more targets in higher tiers, we need to spend more runs of observations than if we observe them in lower tiers. The present selection method, though made arbitrarily, remains open to adjustment in accordance with the guidance provided in the Ariel Red Book [Tinetti et al., 2021].

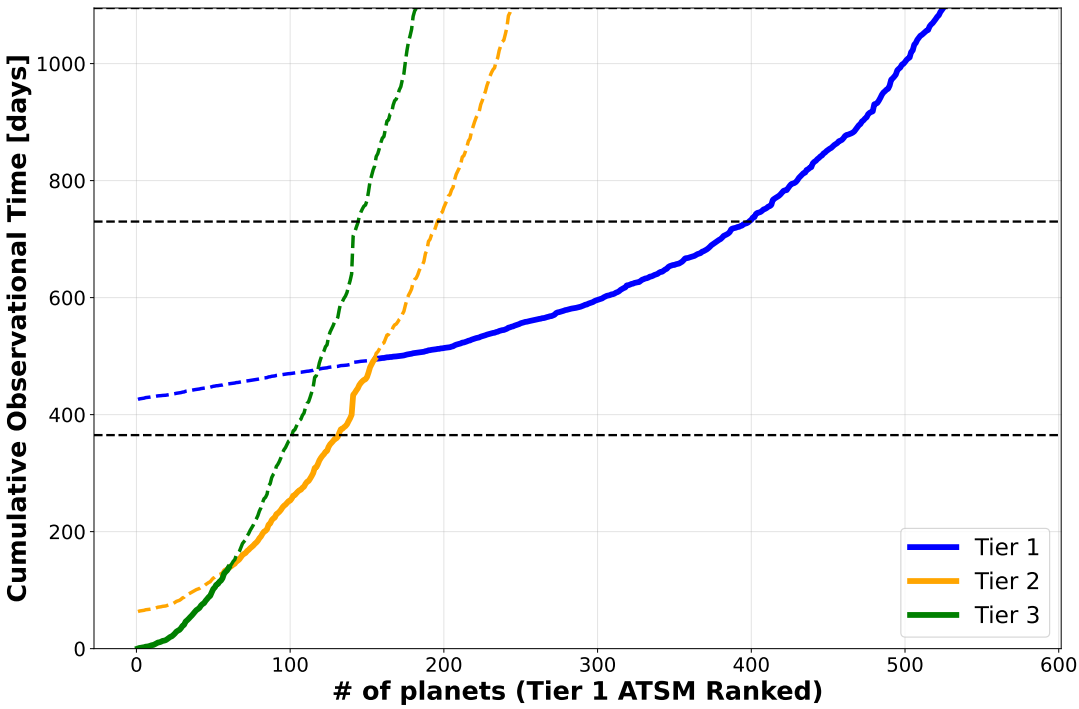

Figure 24: The number of targets observable within 3 years time frame in three different tiers. The top 60 ATSM planets are selected to be Tier 3 (green), Tier 2 targets are the next 95 targets observable within 365 days (orange), and the rest is 369 targets in Tier 1 (blue). The dashed line trace out the cumulative time needed if we want to observe more/fewer targets in each tier.

In comparison to all JWST planned and completed transit targets, the potential Ariel

transit targets focus on longer transiting duration for rocky planets, sub-Neptunes, and Neptunes, as shown in Figure 25. For gas giants, the optimal targets clustered between planets with transits between 2 - 6 hours, not accounting for in-and-out baseline durations. Figure 26 and 27 demonstrated the radius, period, and transit duration distribution of those targets. We see a range of planet diversity in different tiers as indicated by their shape. Most transit observation duration is less than five hours, accounting for in-and-out baseline. The lowest ATSM in Tier 1 drops to 2, indicating around $\sim$ 10 time of observation might be required to yield a high enough resolution. Nevertheless, our transit target selection completes a comprehensive characterization of a diverse range of planets within a practical time span of three years and fills the observational gap pertaining to rocky and (sub) Neptune planets that might be lacking in the phase curve observations.

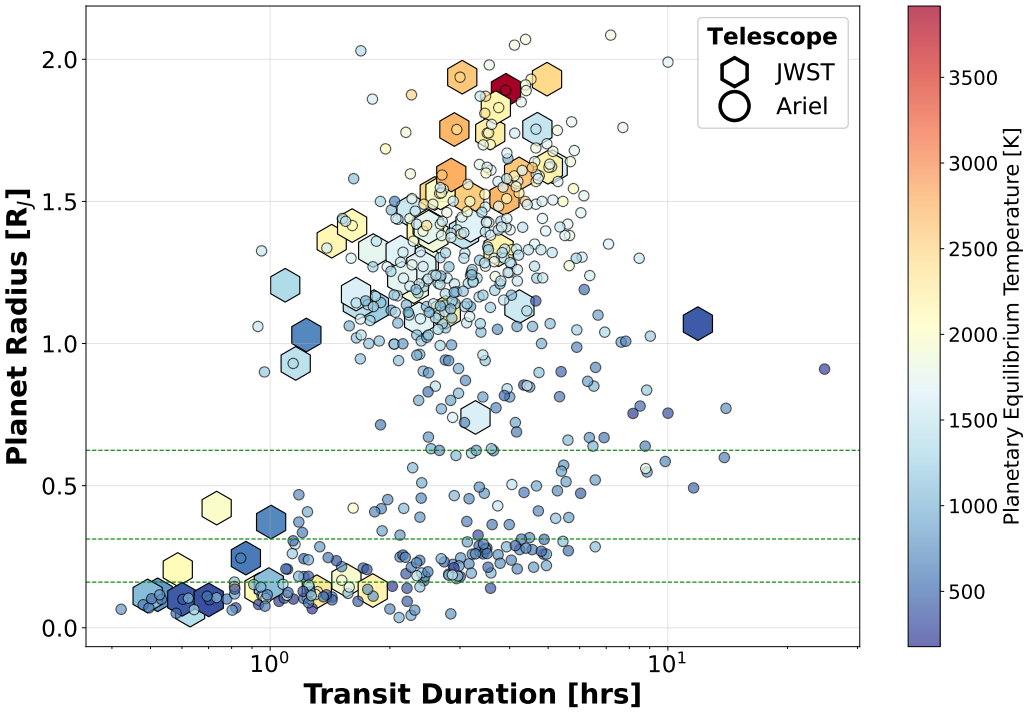

Figure 25: The distribution of radius and transit duration (not accounting baseline) of 524 potential Ariel transit targets (following Figure 24) and 355 JWST transit targets (planned and done). The longest transit can be up to 20 hours, with most clustered between 2 - 6 hours.

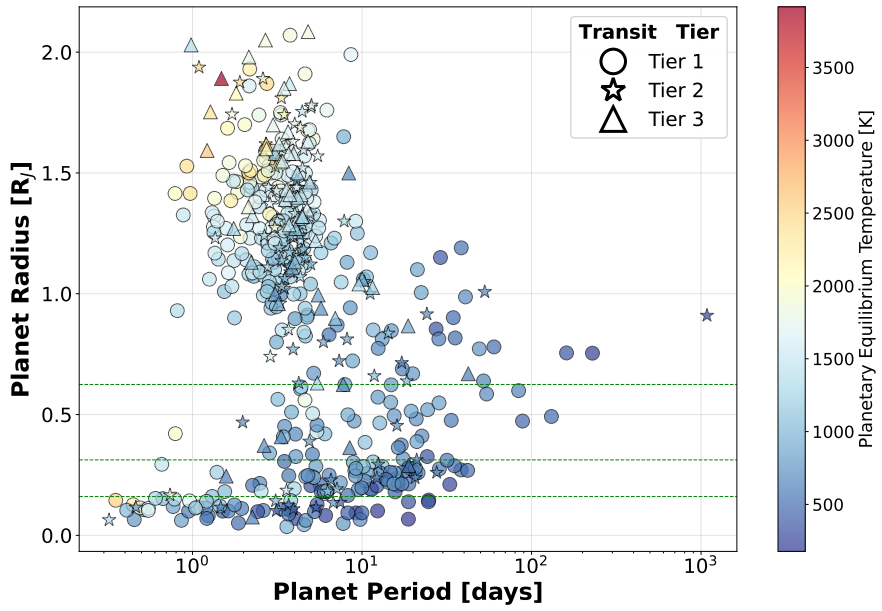

(a) The distribution of radius and orbital period of 524 targets we selected for transit spectroscopy in each three tiers. The targets are diverse in planetary radius across all tiers.

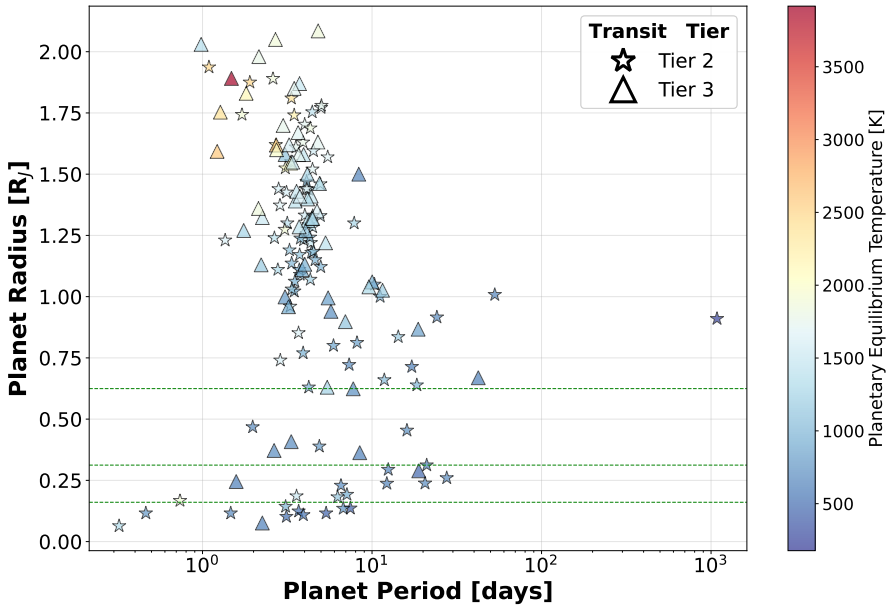

(b) The distribution of radius and orbital period of 155 targets we selected for transit spectroscopy in Tier 1 & 2. A high proportion of targets are gas giants.

Figure 26: Targets selected for Ariel Transmission spectroscopy based on their ranked Ariel Transmission Spectroscopy Metric (ATSM). **Top:** Targets in each of the three tiers. **Bottom:** Targets with higher signals that are in Tier 2 & 3.

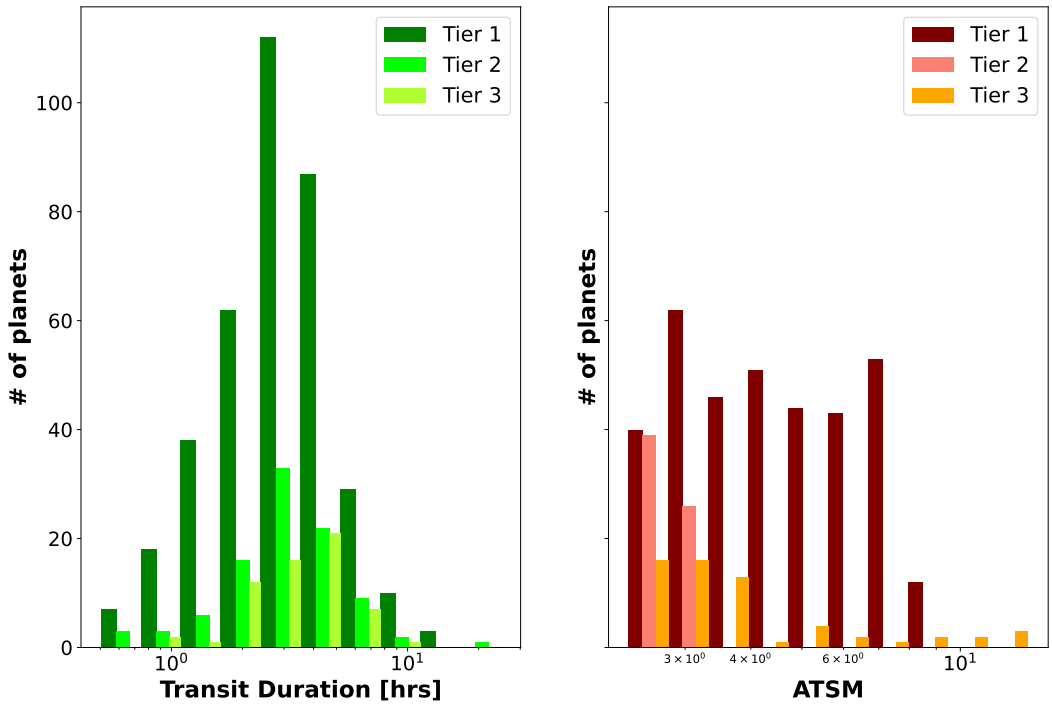

Figure 27: Histogram of the distribution of 524 targets selected based on Ranked ATSM Method as a function of transit period (including in-and-out-baseline; green), and the ATSM (red). Most targets have a transit observation duration of 5 hours. The lowest ATSM in Tier 1 is around 2.

4.2 Best in Bins Method

The method employed by Edwards et al. [2019] to select transit and eclipse targets divides all potential planets based on their host star's effective temperature, planetary radius, and planetary equilibrium temperature. There are in total 14 different bins, as listed in Table 4, and at least two planets within each bin need to be contained within the final target list. Here, we follow this methodology and modify our previous target list if it doesn't satisfy our requirements.

As shown in Figure 28, our target list for transit satisfies the binning requirement listed in Table 4. However, when adopting a three-dimensional criteria for these requisites, numerous bins are found to be absent. Further inquiry is necessary following communication with Edwards.

Parameter	Class	Bounds
Stellar Effective Temperature	M	$T_s < 3955K$
	K	3955 K $< T_s <$ 5330 K
	G	5330 K $< Ts <$6070 K
	F	6070 K $< Ts <$ 7200 K
Planetary Radius	Earth/super-Earth	$R_p < 0.161R_J$
	Sub-Neptune	$0.161R_J < R_p < 0.312R_J$
	Neptune	$0.312R_J < R_p < 0.535R_J$
	Jupiter	$0.535R_J < R_p > 1.427R_J$
	Massive Jupiter	$R_p > 1.427R_J$
Planetary Equilibrium Temperature	Temperature/ Warm	$T_p < 500K$
	Very Warm	500 K $< T_p <$ 1000 K
	Hot	1000 K $< T_p <$ 1500 K
	Very Hot	1500 K $< T_p <$ 2500 K
	Ultra Hot	$T_p >$ 2500 K

Table 4: The bounds used to classify potential targets for Ariel mission to ensure a diverse population of planets are characterized. Table adopted from Edwards et al. [2019].

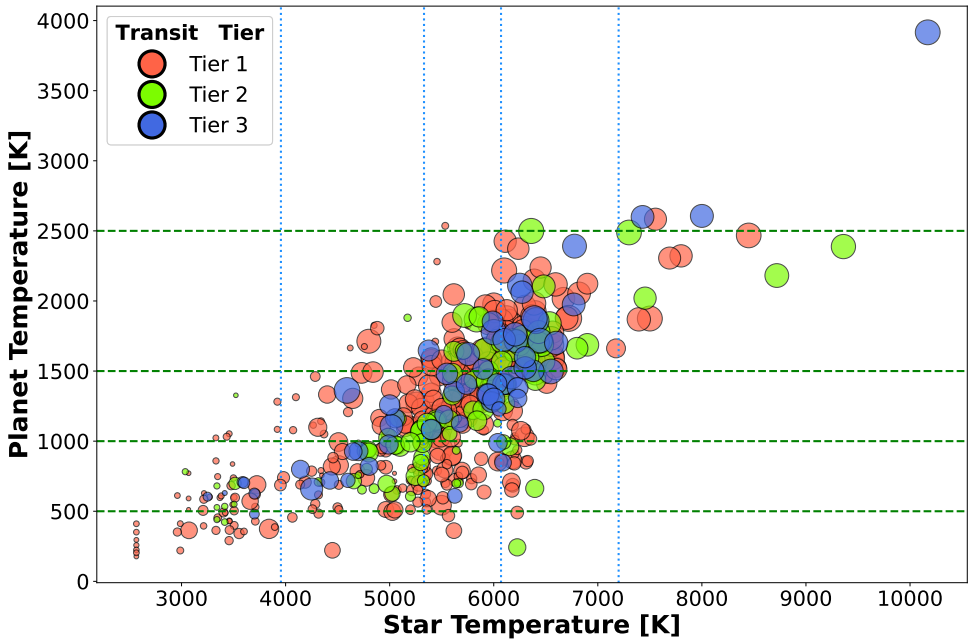

Figure 28: The distribution of stellar effective temperature and planetary equilibrium temperature of the 524 targets we selected in section 4.1. The size of the plot scales with the planet radius. The vertical blue lines and the horizontal green lines divide the planets into bins in accordance with Table 4. Our selection satisfy Edwards' condition that at least two planets in each bins needs to be included.

5 Notional Scheduler

The mission planning of Ariel remains a major challenge before its launch as it is crucial in determining the maximum scientific outcome of the entire mission. An optimal scheduler of a mission will not only consider the best targets to observe, and the time spent on each target, but also the calibration, maintenance, slew of telescope, and maximum use of gap hours (revisits, back-up targets, ancillary science). Morales et al. [2022] have utilized Evolutionary Algorithms (EAs) to schedule the observation of $\sim$ 1000 targets from Edwards et al. [2019] during Ariel's lifetime including transits, eclipses, and phase curves. They found that up to $85 - 90\%$ of Ariel's mission time can be dedicated to science. Additionally, they computed that the observation of phase curve can significantly improve observation efficiency by reducing the amount of waiting time in between targets, at the expense of shortening Tier 1 target list. Figure 29 shows the sky location of the 51 Tier 2 AESM targets and 524 Tier 1 transmission targets we selected. The targets that we selected are well distributed among the sky, facilitating scheduling and observational planning. We leave the exact scheduling of all Ariel targets as future investigation.

6 Conclusion

Phase curve observations are powerful technics to characterize the atmospheric properties, thermal structure, and chemical composition of exoplanets. This updated study improves on the previous phase curve framework from Charnay et al. [2021] by creating our own Figure of Merit (FoM). We select a total of 51 primary phase curve targets from the Ariel short list given by Edwards et al. [2019]. Those targets are observable within 140 days, corresponding to $\sim 10\%$ of total Ariel science time. According to our study, we found that the selection of giant planets yields the highest scientific return in a target-limited regime, encompassing all of our new list of 51 targets. For smaller planets, the best strategy is to work complementarily with other telescopes such as JWST and PLATO, which boasts higher resolutions and already observed a dozen of terrestrial planets. It is likely that JWST would complete more than 50 phase curve observations of terrestrial planets or (sub) Neptunes before the launch of Ariel.

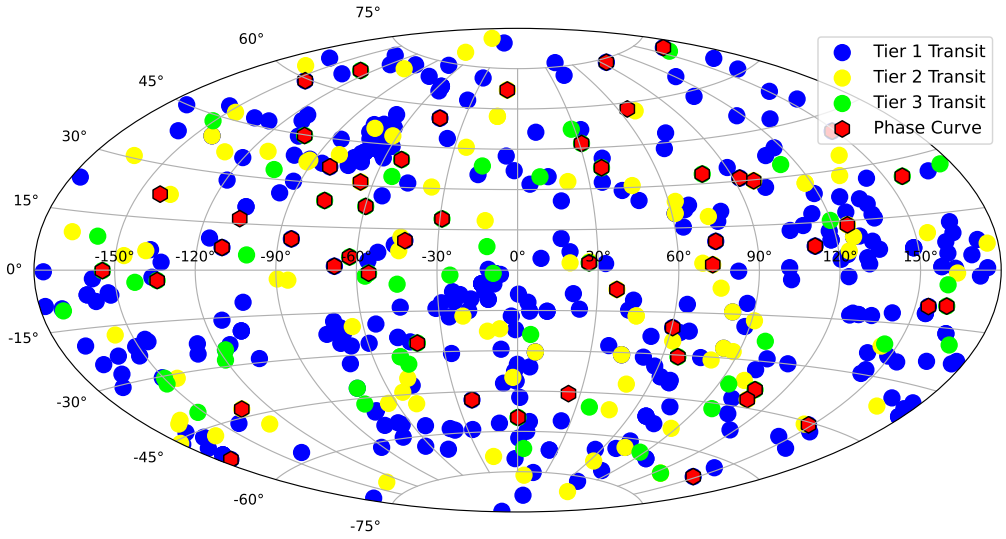

Figure 29: Sky location of the 51 Tier 2 AESM targets (red) and 106 Tier 1 targets with ATSM > 10 (blue). Their even distribution in the night sky is advantageous to scheduling individual observations.

In addition, we also take into consideration of a partial phase curve observation, which looks at a minimum of 45° before and after the eclipse to cover the phase curve offset due to heat transport. This method effectively reduces the observational duration for planets with long orbital periods ($>$ 48 hours). Within a 365-day phase curve observation period, it is possible to observe 36 full phase curves and 99 partial phase curves targets ($\pm$45°). Those targets serve as excellent backup options if additional phase curve science time is allocated.

Furthermore, we selected a preliminary list of 524 transit targets based on the Ariel Transmission spectroscopy Metric (ATSM) we constructed. Among those targets, 60 targets reach Tier 3 resolution, 95 reach Tier 2, and 369 reach Tier 1 resolution within a three-year observation timeframe. Together with the one-year notional observational time allocated to phase curve, we expect to characterize more than 550 targets in four years, including planets in all radius ranges. We leave the work of constructing a notional scheduling of those selected Ariel targets for future studies.

A

Table 5: 43 selected targets for phase curve observations using the Best in Class (section 3.1). The solid horizontal line separates planets into terrestrial planets (6), sub-Neptune (6), Neptune (6), and gas giants (25).

Planet Name	**Planet Radius** $[R_J]$	**Orbital Period [days]**	**Planet Temperature [K]**	**Tier2 AESM**
HD 219134 b	0.143	3.092926	983.3417771	0.619
TOI-431 b	0.114	0.490047	1825.985174	0.473
HD 3167 b	0.143	0.959622	1710.225966	0.422
LHS 3844 b	0.116	0.46292913	782.2536742	0.362
GJ 367 b	0.064	0.321962	1327.049329	0.354
GJ 9827 b	0.141	1.2089819	1142.158053	0.326
55 Cnc e	0.167	0.7365474	1880.057222	2.439
K2-266 b	0.294	0.658524	1461.13458	0.884
HR 858 b	0.186	3.58599	1509.965895	0.603
pi Men c	0.182	6.2679	1128.309313	0.568
GJ 1214 b	0.245	1.58040433	603.9487151	0.540
TOI-824 b	0.261	1.392978	1207.388375	0.481
LTT 9779 b	0.421	0.792052	1996.286523	2.750
GJ 436 b	0.372	2.64388312	708.0229527	1.740
DS Tuc A b	0.509	8.138268	879.83315	1.189
AU Mic b	0.363	8.463	626.4279341	1.093
K2-39 b	0.56	4.60543	1806.045712	0.813
TOI-674 b	0.468	1.977143	698.8670804	0.777
HIP 65 A b	2.03	0.9809734	1361.757722	49.014
KELT-9 b	1.891	1.4811235	3916.236076	34.597
WASP-33 b	1.593	1.21987	2599.597377	31.680
WASP-189 b	1.619	2.724033	2606.643375	30.308
HD 189733 b	1.13	2.21857567	1162.930605	28.587
KELT-20 b	1.741	3.4741085	2181.396627	22.059
HD 209458 b	1.39	3.52474859	1405.91027	21.356
WASP-76 b	1.83	1.809886	2110.974286	18.482
WASP-18 b	1.24	0.94145223	2408.746207	17.852
MASCARA-1 b	1.5	2.14878	2583.193818	15.999
WASP-121 b	1.753	1.27492504	2391.043885	15.942
KELT-7 b	1.6	2.73477	1975.133011	15.048
MASCARA-4 b	1.53	2.82406	2321.685164	14.895
TOI-1518 b	1.875	1.902603	2488.500269	14.794
XO-6 b	2.07	3.7650007	1875.839925	13.699
WASP-77 A b	1.23	1.36002854	1640.556222	13.219
WASP-12 b	1.937	1.09142	2499.272484	12.557
HD 202772 A b	1.545	3.308958	2062.654694	12.451
HAT-P-32 b	1.98	2.1500082	1777.378359	12.315
TOI-1431 b	1.49	2.650237	2306.103917	12.233
HAT-P-70 b	1.87	2.74432452	2467.441219	11.618
TOI-2109 b	1.347	0.67247414	3049.33241	11.335
XO-3 b	1.41	3.19154	1977.826146	10.779
KELT-11 b	1.35	4.7361	1646.55533	10.773
KELT-4 A b	1.699	2.9895932	1761.948781	9.678

B

Table 6: 51 potential Ariel phase curve targets selected via the Ranked FoM Method (section 3.2) that has Tier 2 Ariel Emission Spectroscopy Metric (AESM) > 7.

Planet Name	**Planet Radius** $[R_J]$	**Orbital Period [days]**	**Planet Temperature [K]**	**Tier2 AESM**
HIP 65 A b	2.03	0.9809734	1361.757722	49.014
KELT-9 b	1.891	1.4811235	3916.236076	34.597
WASP-33 b	1.593	1.21987	2599.597377	31.680
WASP-189 b	1.619	2.724033	2606.643375	30.308
HD 189733 b	1.13	2.21857567	1162.930605	28.587
KELT-20 b	1.741	3.4741085	2181.396627	22.059
HD 209458 b	1.39	3.52474859	1405.91027	21.356
WASP-76 b	1.83	1.809886	2110.974286	18.482
WASP-18 b	1.24	0.94145223	2408.746207	17.852
MASCARA-1 b	1.5	2.14878	2583.193818	15.999
WASP-121 b	1.753	1.27492504	2391.043885	15.942
KELT-7 b	1.6	2.73477	1975.133011	15.048
MASCARA-4 b	1.53	2.82406	2321.685164	14.895
TOI-1518 b	1.875	1.902603	2488.500269	14.794
XO-6 b	2.07	3.7650007	1875.839925	13.699
WASP-77 A b	1.23	1.36002854	1640.556222	13.219
WASP-12 b	1.937	1.09142	2499.272484	12.557
HD 202772 A b	1.545	3.308958	2062.654694	12.451
HAT-P-32 b	1.98	2.1500082	1777.378359	12.315
TOI-1431 b	1.49	2.650237	2306.103917	12.233
HAT-P-70 b	1.87	2.74432452	2467.441219	11.618
TOI-2109 b	1.347	0.67247414	3049.33241	11.335
XO-3 b	1.41	3.19154	1977.826146	10.779
KELT-11 b	1.35	4.7361	1646.55533	10.773
KELT-4 A b	1.699	2.9895932	1761.948781	9.678
WASP-74 b	1.36	2.13775	1853.119534	9.647
KELT-23 A b	1.323	2.255251	1514.89041	9.624
KELT-14 b	1.743	1.7100566	1896.413932	9.435
WASP-82 b	1.62	2.70579	2104.095408	9.419
WASP-103 b	1.528	0.925542	2425.974311	9.329
KELT-8 b	1.62	3.24406	1621.405269	9.253
WASP-14 b	1.38	2.24375	1799.902126	9.053
WASP-19 b	1.415	0.78883852	2046.376552	9.039
KELT-19 A b	1.91	4.6117093	1874.7186	8.948
KELT-17 b	1.525	3.0801716	2019.861101	8.893
KELT-2 A b	1.35	4.11379	1701.497909	8.668
HAT-P-67 b	2.085	4.8101025	1860.033202	8.638
HAT-P-41 b	2.05	2.69405	1873.807621	8.555
KELT-24 b	1.272	5.5514926	1413.610529	8.396
WASP-178 b	1.81	3.3448285	2388.0138	8.167
WASP-79 b	1.67	3.66238	1700.784189	7.788
WASP-140 b	1.44	2.2359835	1272.734581	7.681
CoRoT-2 b	1.466	1.7429935	1496.310943	7.586
WASP-3 b	1.42	1.84683	1925.257547	7.561
KELT-3 b	1.56	2.70339	1757.994489	7.494
WASP-54 b	1.58	3.69364	1722.740162	7.417

Continued on next page

WASP-87 b	1.385	1.682795	2238.559601	7.323
WASP-95 b	1.23	2.18467	1559.394901	7.279
KELT-18 b	1.57	2.8717518	2015.929666	7.146
HAT-P-57 b	1.74	2.4653	1792.567196	7.115
WASP-43 b	0.93	0.813475	1332.594418	7.037

References

T. J. Bell, L. Dang, N. B. Cowan, J. Bean, J.-M. Désert, J. J. Fortney, D. Keating, E. Kempton, L. Kreidberg, M. R. Line, M. Mansfield, V. Parmentier, K. B. Stevenson, M. Swain, and R. T. Zellem. A comprehensive reanalysis of ispitzer/i's 4.5 m phase curves, and the phase variations of the ultra-hot jupiters MASCARA-1b and KELT-16b. *Monthly Notices of the Royal Astronomical Society*, 504(3):3316–3337, Apr. 2021. doi: 10.1093/mnras/stab1027. URL https://doi.org/10.1093/mnras/stab1027.

C. Broeg, A. Fortier, D. Ehrenreich, Y. Alibert, W. Baumjohann, W. Benz, M. Deleuil, M. Gillon, A. Ivanov, R. Liseau, M. Meyer, G. Oloffson, I. Pagano, G. Piotto, D. Pollacco, D. Queloz, R. Ragazzoni, E. Renotte, M. Steller, and N. T. and. CHEOPS: A transit photometry mission for ESA's small mission programme. *EPJ Web of Conferences*, 47:03005, 2013. doi: 10.1051/epjconf/20134703005. URL https://doi.org/10.1051/epjconf/20134703005.

B. Charnay, J. M. Mendonça, L. Kreidberg, N. B. Cowan, J. Taylor, T. J. Bell, O. Demangeon, B. Edwards, C. A. Haswell, G. Morello, L. V. Mugnai, E. Pascale, G. Tinetti, P. Tremblin, and R. T. Zellem. A survey of exoplanet phase curves with ariel. *Experimental Astronomy*, 53 (2):417–446, Mar. 2021. doi: 10.1007/s10686-021-09715-x. URL https://doi.org/10.1007/s10686-021-09715-x.

N. B. Cowan, T. Greene, D. Angerhausen, N. E. Batalha, M. Clampin, K. Colón, I. J. M. Crossfield, J. J. Fortney, B. S. Gaudi, J. Harrington, N. Iro, C. F. Lillie, J. L. Linsky, M. Lopez-Morales, A. M. Mandell, and K. B. S. and. Characterizing transiting planet atmospheres through 2025. *Publications of the Astronomical Society of the Pacific*, 127(949):311–327, Mar. 2015. doi: 10.1086/680855. URL https://doi.org/10.1086/680855.

B. Edwards, L. Mugnai, G. Tinetti, E. Pascale, and S. Sarkar. An updated study of potential targets for ariel. *The Astronomical Journal*, 157(6):242, May 2019. doi: 10.3847/1538-3881/ab1cb9. URL https://doi.org/10.3847/1538-3881/ab1cb9.

E. M.-R. Kempton, J. L. Bean, D. R. Louie, D. Deming, D. D. B. Koll, M. Mansfield, J. L. Christiansen, M. López-Morales, M. R. Swain, R. T. Zellem, S. Ballard, T. Barclay, J. K. Barstow, N. E. Batalha, T. G. Beatty, Z. Berta-Thompson, J. Birkby, L. A. Buchhave, D. Charbonneau, N. B. Cowan, I. Crossfield, M. de Val-Borro, R. Doyon, D. Dragomir, E. Gaidos, K. Heng, R. Hu, S. R. Kane, L. Kreidberg, M. Mallonn, C. V. Morley, N. Narita, V. Nascimbeni, E. Pallé, E. V. Quintana, E. Rauscher, S. Seager, E. L. Shkolnik, D. K. Sing, A. Sozzetti, K. G. Stassun, J. A. Valenti, and C. von Essen. A framework for prioritizing the iTESS/i planetary candidates most amenable to atmospheric characterization. *Publications of the Astronomical Society of the Pacific*, 130(993):114401, Sept. 2018. doi: 10.1088/1538-3873/aadf6f. URL https://doi.org/10.1088/1538-3873/aadf6f.

J. Morales, N. Nakhjiri, J. Colomé, I. Ribas, E. García, D. Moreno, and F. Vilardell. Ariel mission planning. *Experimental Astronomy*, 53(2):807–829, Jan. 2022. doi: 10.1007/s10686-021-09822-9. URL https://doi.org/10.1007/s10686-021-09822-9.

L. V. Mugnai, E. Pascale, B. Edwards, A. Papageorgiou, and S. Sarkar. ArielRad: the ariel radiometric model. *Experimental Astronomy*, 50(2-3):303–328, Oct. 2020. doi: 10.1007/s10686-020-09676-7. URL https://doi.org/10.1007/s10686-020-09676-7.

L. V. Mugnai, A. Al-Refaie, A. Bocchieri, Q. Changeat, E. Pascale, and G. Tinetti. Alfnoor: Assessing the information content of ariel's low-resolution spectra with planetary population studies. *The Astronomical Journal*, 162(6):288, Dec. 2021. doi: 10.3847/1538-3881/ac2e92. URL https://doi.org/10.3847/1538-3881/ac2e92.

V. Parmentier and I. J. M. Crossfield. Exoplanet phase curves: Observations and theory. In *Handbook of Exoplanets*, pages 1419–1440. Springer International Publishing, 2018. doi: 10.1007/978-3-319-55333-7_116. URL https://doi.org/10.1007/978-3-319-55333-7_116.

J. Penn and G. K. Vallis. Atmospheric circulation and thermal phase-curve offset of tidally and nontidally locked terrestrial exoplanets. *The Astrophysical Journal*, 868(2):147, Dec. 2018. doi: 10.3847/1538-4357/aaeb20. URL https://doi.org/10.3847/1538-4357/aaeb20.

W. Pluriel. Hot exoplanetary atmospheres in 3d. *Remote Sensing*, 15(3):635, Jan. 2023. doi: 10.3390/rs15030635. URL https://doi.org/10.3390/rs15030635.

H. Rauer, C. Aerts, J. Cabrera, and P. Team. The PLATO mission. *Astronomische Nachrichten*, 337(8-9):961–963, Sept. 2016. doi: 10.1002/asna.201612408. URL https://doi.org/10.1002/asna.201612408.

G. Tinetti, T. Encrenaz, and A. Coustenis. Spectroscopy of planetary atmospheres in our galaxy. *The Astronomy and Astrophysics Review*, 21(1), Oct. 2013. doi: 10.1007/s00159-013-0063-6. URL https://doi.org/10.1007/s00159-013-0063-6.

G. Tinetti, P. Eccleston, C. Haswell, P.-O. Lagage, J. Leconte, T. Lüftinger, G. Micela, M. Min, G. Pilbratt, L. Puig, M. Swain, L. Testi, D. Turrini, B. Vandenbussche, M. R. Z. Osorio, A. Aret, J.-P. Beaulieu, L. Buchhave, M. Ferus, M. Griffin, M. Guedel, P. Hartogh, P. Machado, G. Malaguti, E. Pallé, M. Rataj, T. Ray, I. Ribas, R. Szabó, J. Tan, S. Werner, F. Ratti, C. Scharmberg, J.-C. Salvignol, N. Boudin, J.-P. Halain, M. Haag, P.-E. Crouzet, R. Kohley, K. Symonds, F. Renk, A. Caldwell, M. Abreu, G. Alonso, J. Amiaux, M. Berthé, G. Bishop, N. Bowles, M. Carmona, D. Coffey, J. Colomé, M. Crook, L. Désjonqueres, J. J. Díaz, R. Drummond, M. Focardi, J. M. Gómez, W. Holmes, M. Krijger, Z. Kovacs, T. Hunt, R. Machado, G. Morgante, M. Ollivier, R. Ottensamer, E. Pace, T. Pagano, E. Pascale, C. Pearson, S. M. Pedersen, M. Pniel, S. Roose, G. Savini, R. Stamper, P. Szirovicza, J. Szoke, I. Tosh, F. Vilardell, J. Barstow, L. Borsato, S. Casewell, Q. Changeat, B. Charnay, S. Civiš, V. C. d. Foresto, A. Coustenis, N. Cowan, C. Danielski, O. Demangeon, P. Drossart, B. N. Edwards, G. Gilli, T. Encrenaz, C. Kiss, A. Kokori, M. Ikoma, J. C. Morales, J. Mendonça, A. Moneti, L. Mugnai, A. G. Muñoz, R. Helled, M. Kama, Y. Miguel, N. Nikolaou, I. Pagano, O. Panic, M. Rengel, H. Rickman, M. Rocchetto, S. Sarkar, F. Selsis, J. Tennyson, A. Tsiaras, O. Venot, K. Vida, I. P. Waldmann, S. Yurchenko, G. Szabó, R. Zellem, A. Al-Refaie, J. P. Alvarez, L. Anisman, A. Arhancet, J. Ateca, R. Baeyens, J. R. Barnes, T. Bell, S. Benatti, K. Biazzo, M. Błecka, A. S. Bonomo, J. Bosch, D. Bossini, J. Bourgalais, D. Brienza, A. Brucalassi, G. Bruno, H. Caines, S. Calcutt, T. Campante, R. Canestrari, N. Cann, G. Casali, A. Casas, G. Cassone, C. Cara, M. Carmona, L. Carone, N. Carrasco, Q. Changeat, P. Chioetto, F. Cortecchia, M. Czupalla, K. L. Chubb, A. Ciaravella, A. Claret, R. Claudi, C. Codella, M. G. Comas, G. Cracchiolo, P. Cubillos, V. Da Peppo, L. Decin, C. Dejabrun, E. Delgado-Mena, A. Di Giorgio, E. Diolaiti, C. Dorn, V. Doublier, E. Doumayrou, G. Dransfield, L. Dumaye, E. Dunford, A. J. Escobar, V. Van Eylen, M. Farina, D. Fedele, A. Fernández, B. Fleury, S. Fonte, J. Fontignie, L. Fossati, B. Funke, C. Galy, Z. Garai, A. García, A. García-Rigo, A. Garufi, G. G. Sacco, P. Giacobbe,

A. Gómez, A. Gonzalez, F. Gonzalez-Galindo, D. Grassi, C. Griffith, M. G. Guarcello, A. Goujon, A. Gressier, A. Grzegorczyk, T. Guillot, G. Guilluy, P. Hargrave, M.-L. Hellin, E. Herrero, M. Hills, B. Horeau, Y. Ito, N. C. Jessen, P. Kabath, S. Kálmán, Y. Kawashima, T. Kimura, A. Knížek, L. Kreidberg, R. Kruid, D. J. M. Kruijssen, P. Kubelík, L. Lara, S. Lebonnois, D. Lee, M. Lefevre, T. Lichtenberg, D. Locci, M. Lombini, A. S. Lopez, A. Lorenzani, R. MacDonald, L. Magrini, J. Maldonado, E. Marcq, A. Migliorini, D. Modirrousta-Galian, K. Molaverdikhani, S. Molinari, P. Mollière, V. Moreau, G. Morello, G. Morinaud, M. Morvan, J. I. Moses, S. Mouzali, N. Nakhjiri, L. Naponiello, N. Narita, V. Nascimbeni, A. Nikolaou, V. Noce, F. Oliva, P. Palladino, A. Papageorgiou, V. Parmentier, G. Peres, J. Pérez, S. Perez-Hoyos, M. Perger, C. C. Pestellini, A. Petralia, A. Philippon, A. Piccialli, M. Pignatari, G. Piotto, L. Podio, G. Polenta, G. Preti, T. Pribulla, M. L. Puertas, M. Rainer, J.-M. Reess, P. Rimmer, S. Robert, A. Rosich, L. Rossi, D. Rust, A. Saleh, N. Sanna, E. Schisano, L. Schreiber, V. Schwartz, A. Scippa, B. Seli, S. Shibata, C. Simpson, O. Shorttle, N. Skaf, K. Skup, M. Sobiecki, S. Sousa, A. Sozzetti, J. Šponer, L. Steiger, P. Tanga, P. Tackley, J. Taylor, M. Tecza, L. Terenzi, P. Tremblin, A. Tozzi, A. Triaud, L. Trompet, S.-M. Tsai, M. Tsantaki, D. Valencia, A. C. Vandaele, M. Van der Swaelmen, A. Vardan, G. Vasisht, A. Vazan, C. Del Vecchio, D. Waltham, P. Wawer, T. Widemann, P. Wolkenberg, G. H. Yip, Y. Yung, M. Zilinskas, T. Zingales, and P. Zuppella. Ariel: Enabling planetary science across light-years, 2021. URL `https://arxiv.org/abs/2104.04824`.